RL-81-019

Rutherford and Appleton Laboratories
CHILTON, DIDCOT, OXON, OX11 0QX

Neutron Spin Echo Spectroscopy on the Spallation Neutron Source

J Penfold and W G Williams

February 1981

RL-81-019

RL-81-019

NEUTRON SPIN ECHO SPECTROSCOPY ON THE SPALLATION NEUTRON SOURCE

J Penfold and W G Williams

Abstract

An investigation has been made into the practicability of combining the neutron spin echo and time-of-flight techniques on the Rutherford Laboratory Spallation Neutron Source. Preliminary specifications are presented for a quasielastic instrument with an energy resolution down to $\sim$ 10 neV and an inelastic spectrometer for measuring excitation widths $\sim$ 1 μeV.

Neutron Division
Rutherford and Appleton Laboratories
Chilton, Didcot, Oxon OX11 0QX.

February 1981

CONTENTS

		Page
1.	INTRODUCTION	1
2.	PRINCIPLE OF THE SPIN ECHO TECHNIQUE	2
3.	SCIENCE	7
	3.1 Quasielastic Scattering	7
	3.2 Inelastic Scattering	9
4.	SPECIFICATION FOR A QUASIELASTIC SCATTERING INSTRUMENT	10
5.	SPECIFICATION FOR AN INELASTIC SCATTERING INSTRUMENT	25
	ACKNOWLEDGEMENTS	31
	TABLES	32
	FIGURE CAPTIONS	36
	REFERENCES	37

1. INTRODUCTION

The neutron spin echo (NSE) technique for high resolution inelastic neutron scattering is a relatively new technique, and was introduced by Mezei[1] in 1972.

In conventional inelastic neutron scattering the energy change on scattering is deduced by selecting the incident and scattered neutron energies. High energy resolution implies good monochromation and a resultant reduction in neutron intensity. In the neutron spin echo technique the energy change on scattering is measured directly as a change in the precessing polarisation of the neutron spin.

The spin echo technique is described in detail elsewhere[1-12]. The main advantages of the technique are:

(i) Energy resolution and monochromation are, in principle, decoupled, resulting in good neutron economy.

(ii) Energy resolutions of the order of ten times better than that obtained using other techniques are achievable.

(iii) The intermediate scattering law $S(\underline{Q},t)$ is measured directly.

(iv) Resolution corrections are applied by a simple division, rather than by a deconvolution.

The spin echo technique was first developed on the IN11 instrument[13,14] at the Institut Laue Langevin (ILL) where it is combined with a classical long wavelength basic spectrometer to provide conventional momentum transfer resolutions (10 to 20%) for high energy resolution quasielastic studies[3,4]. It is also proposed to combine the spin echo technique with a triple axis basic spectrometer for the study of elementary excitations with high energy resolution[3,9,11,12]. More recently Mezei[15] has

proposed using the spin echo technique on a pulsed neutron source, that is on a time-of-flight spectrometer. In discussing the practical consequences of combining the spin echo and time-of-flight techniques on the Rutherford Laboratory Spallation Neutron Source (SNS), extensive use will be made of the method suggested by Mezei[15]. In order to utilise the main advantages of the time-of-flight technique on a pulsed source we require,

(i) a maximum incident wavelength band, $\Delta\lambda$, and
(ii) a large detetor solid angle, implying the use of a multi-detector.

The length of the instrument, its distance from the source, and the pulse repetition frequency of the source will determine the maximum wavelength band $\Delta\lambda$ that can be used without frame overlap.

The possibility of phasing the spin turn coils with the SNS pulse means that the degradation of the spin echo signal which occurs on steady state sources for poorly monochromatic beams due to the wavelength dependent action of the spin turn coils, can be avoided or at least minimised. In most pulsed source spin echo instruments the resolution in the scattering vector Q ($\Delta Q/Q$) will in general be dominated by $\Delta\theta/\theta$, the uncertainty in defining the scattering angle, rather than the uncertainty in determining the neutron wavelength, $\delta\lambda/\lambda = \delta T/T$. This should allow better $\Delta Q/Q$'s to be achieved than on steady state source instruments where the $\delta\lambda/\lambda$ contribution to the Q resolution is often significant.

In this paper the principles of the spin echo technique are briefly reviewed. The scientific case for providing spin echo on the SNS is then discussed and specifications presented for both quasielastic and inelastic spectrometers.

2. PRINCIPLE OF THE NEUTRON SPIN ECHO TECHNIQUE

Detailed descriptions of the spin-echo technique are presented elsewhere[1-15]; we will consider here the main principles only,

and discuss briefly its application to studying quasielastic and inelastic processes, particularly in combination with the time-of-flight method.

In the neutron spin echo technique a neutron polarised perpendicular to the magnetic field direction traverses a well-defined field region, in which it performs a precession through Ω_o radians. The neutron spin is then flipped, that is, the polarisation direction is turned about an axis perpendicular to the field direction. The neutron spin then enters a second field region where it undergoes a precession through Ω_1 radians which appear to be in the opposite sense to the Ω_o Precessions. Let us first consider the experiment where the sample is placed at the spin flipper position and the scattering is purely elastic. If the field integrals experienced before and after the sample are identical, then the precessional phase shift $\Omega_o - \Omega_1 = 0$. This is the so-called "focussed" echo condition, where the measured polarisation is a maximum. Inelastic processes give $\Omega_o \neq \Omega_1$ that is a measured polarisation which is less than the maximum.

The resultant change in the Larmor precession angle for the generalised case of inelastic scattering and non-identical field integrals before and after the scattering is[3]

$$\Omega = \Omega_o - \Omega_1 = \gamma_L \left[\frac{\ell_o H_o}{v_1} - \frac{\ell_1 H_1}{v_1}\right] \qquad (2.1)$$

where $\gamma_L = 2.916$ kHz/Oe is the Larmor precession constant for neutrons, ℓ and H refer to the coil lengths and fields, v is the neutron velocity, and the subscripts o and 1 refer to the situation before and after the scattering. The basic idea behind NSE is to use Ω as given by equation (2.1) to measure the energy transfer:

$$\hbar\omega = E_1 - E_o = \tfrac{1}{2} m v_o^2 - \tfrac{1}{2} m v_1^2 \qquad (2.2)$$

on scattering. Since Ω and ω are different functions of v_o and v_1 this is only possible locally with respect to an arbitrarily chosen $\hbar\omega_o$, with

$$\Omega - \bar{\Omega} = t(\omega - \omega_o) \qquad (2.3)$$

where $\bar{\Omega}$ is an average precession angle change corresponding to incident and scattered beams of average velocities v_o and v_1, and t is a proportionality constant. Mezei[3] has shown that this condition can only be satisfied if

$$t = \frac{\gamma_L \hbar \ell_o H_o}{m\bar{v}_o^3} = \frac{\gamma_L \hbar \ell_1 H_1}{m\bar{v}_1^3} \qquad (2.4)$$

and that a further practical consequence is that the incident and scattered beams must be roughly monochromatic. Note that t is independent of the subscripts o and 1 for the incident and scattered beams. The two most useful forms of these expressions are:

$$\frac{\ell_o H_o}{\ell_1 H_1} = \frac{\bar{v}_o^3}{\bar{v}_1^3} \qquad (2.5)$$

which describes the general focussing condition for inelastic scattering (or in fact elastic scattering where $\ell_o H_o = \ell_1 H_1$) and

$$t = \hbar\gamma_L \frac{\ell H}{m\bar{v}^3} = \frac{\hbar\bar{\Omega}}{2\bar{E}} \qquad (2.6)$$

The sample scattering is characterised by the scattering function $S(\underline{Q},\omega)$, which we shall consider at first to depend only on ω. This defines the probability that neutrons are scattered with energy transfer $\hbar\omega$, and consequently determines the distribution of precession angles Ω in the scattered beam. The average analysed polarisation, assuming zero spin-flip scattering, is given by

$$\langle p_y \rangle = p_o \left\langle \cos(\Omega - \bar{\Omega}) \right\rangle = p_o \int_{-\infty}^{+\infty} S(\underline{Q},\omega) \cos[t(\omega-\omega_o)]\, d\omega \qquad (2.7)$$

where p_o represents the maximum instrumental polarisation. Note that NSE measures the polarisation component in the direction of the analyser, here denoted as the y direction.

The significance of ω_o is that the energy transfer $\hbar\omega_o$ determines the centre of the NSE group, and that the $\langle p_y \rangle$

measurement determines $\Omega - \bar{\Omega}$, or $\omega - \omega_o$. For quasielastic scattering a further simplification is possible since $\omega_o = 0$, and ω gives the total energy transfer $\hbar\omega$.

In order to obtain full information about the scattering function $S(\underline{Q},\omega)$, p_y has to be measured at several values of the Fourier parameter t. This is most commonly accomplished by scanning the precession fields H_o and H_1.

The above equations have been extended further to include dispersive elementary excitations. The results will not be discussed in this paper; we simply refer to the original texts[3,9,10,11,12].

Figure 1 shows examples of different $(\underline{Q},\omega)$ relationships for quasielastic and inelastic scattering which may be studied using NSE.

Mezei[15] was the first to describe an instrument which combines the spin echo and time-of-flight techniques. Details were given of its application for measuring quasielastic scattering where the precession field regions before and after the scatterer have identical field intengrals $H_o\ell_o = H_1\ell_1 = H\ell$. In this case the NSE polarisation $\langle p_y \rangle$ depends on the time difference t of the neutron times of flight in the precession fields:

$$t = \ell/v_1 - \ell/v_o \tag{2.8}$$

and this is combined with the total time of flight T:

$$T = \frac{L_1}{v_1} + \frac{L_o}{v_o} \tag{2.9}$$

where L_o and L_1 are the incident and scattered neutron flight paths respectively, to give full information on the scattering process. For quasielastic scattering ($v_1 - v_o \ll v_o$):

$$Q \sim 2\, mv_o \sin\theta/\hbar, \tag{2.10}$$

$$T \sim (L_1 + L_o)/v_o \text{ , and} \tag{2.11}$$

$$\frac{1}{v_1} - \frac{1}{v_o} \sim \frac{v_o - v_1}{v_o^2}$$

$$\sim \frac{\omega\hbar}{mv_o^3} \sim [(2\sin\theta)^3 \cdot \frac{m^2}{\hbar^2 Q^3} \cdot \omega] \tag{2.12}$$

The NSE polarisation measured in a given time-of-flight channel of a detector at fixed scattering angle 2θ is:

$$p_y = p_o \int_{-\infty}^{+\infty} S(\underline{Q},\omega)\, \cos\left(\frac{\gamma_L H\ell}{v_1} - \frac{\gamma_L H\ell}{v_o}\right) d\omega \tag{2.13}$$

$$= p_o \int_{-\infty}^{+\infty} S(\underline{Q},\omega)\, \cos\, [(2\,\mathrm{Sin}\,\theta)^3\, \frac{\gamma_L H\ell m^2}{\hbar^2 Q^3}]\omega . d\omega \tag{2.14}$$

The Fourier time τ is

$$\tau = (2\sin\theta)^3 \cdot \frac{\gamma_L H\ell m^2}{\hbar^2 Q^3} \tag{2.15}$$

Figure 8 shows typical $(\underline{Q},\tau)$ scans for a quasielastic TOF/NSE instrument.

Similar arguments apply to the case of finite energy transfer experiments such as the study of the lifetimes of elementary excitations. As discussed earlier in this section the spin-echo condition corresponding to the velocity change v_o to v_1 is tuned using equation (2.5).

A spin-echo τ scan is usually performed by changing the precession field H. In time-of-flight experiments, however, each detector time channel corresponds to a different Q. It may therefore be possible to scan τ merely by comparing time-of-flight channels belonging to

the same Q at different angles θ (see equation (2.15)), without the need to change the precession coil currents.

3. SCIENCE

In discussing the science possible using the spin echo technique on the SNS, the pattern of research emerging on IN11 will be described. We shall also attempt to identify possible fields of study that may emerge in the future. These will be considered broadly under the headings of either quasielastic or inelastic scattering. The range of studies and the corresponding instrumental requirements are summarised in Tables 1 and 2, and are discussed in more detail below.

3.1 QUASIELASTIC SCATTERING

Neutron spin echo can be used to study relaxation phenomena and diffusive motions at low Q over a large time range and directly in the time domain.

(a) Macromolecular diffusion

Slow diffusive motions may be investigated in a number of macromolecular systems at low Q. Examples include colloidal dispersions (micelles and microemulsions), polymers in solution and melt, and biological systems (for example, haemoglobin, viruses and proteins).

Dynamic small angle neutron spin echo measurements on concentrated colloidal dispersions yield an effective particle diffusion coefficient which is related to the structure factor resulting from interparticle interactions. Such studies on concentrated micellar solutions of sodium dodecyl sulphate have recently been used to provide self-consistent verification of the interpretation of static small angle scattering data[16,17].

Measurements can be performed at low Q to investigate the internal motions of single polymer chains in solution and melt[18-20].

Polymer chain relaxation in solutions of polydimethylsiloxane and polymethylmethacrylate have been investigated. The results largely confirm theoretical predictions.

Quasielastic and inelastic experiments have been used to identify low frequency motions in large biological structures, such as haemoglobin, viruses and proteins[21-23]. Efforts are being directed towards differentiating between translational, rotational diffusion and low frequency collective internal motions ("breathing" modes).

(b) Diffusion in liquid crystals and superionics

High energy resolution is required to measure the small energy broadenings associated with low frequency collective motions in liquid crystals. It has also been proposed that the measurement of the temperature dependence of quasielastic scattering in materials such as $SrCl_2$[22] above the "superionic" transition should show whether the quasielastic scattering is due to anionic diffusion.

(c) Spin relaxation

Much of the recent interest in disordered magnetic systems concerns the spin glass transition and whether or not it is a true phase transition. To test the various models so far proposed it is desirable to measure the dynamics of spin glasses over as large a range as possible; data at low frequencies is particularly important. Using a combination of neutron spin echo and polarisation analysis the time dependent spin correlation function, $S(\underline{Q},t)$, can be measured in the time range 10^{-12} to 10^{-9} sec[24]; this has hitherto been inaccessible to neutrons. The spin dynamics of $Al_2Mn_3Si_3O_{12}$[23] and CuMn[24] have been investigated and yield a broad spectrum of relaxation rates.

(d) Phase transitions

High resolution quasielastic scattering has been used to investigate critical neutron scattering at the nematic-smectic A phase transition

in the compound CB00A[23] where the quasielastic scattering results from fluctuating clusters of the disordered nematic phase.

(e) Diffusion of hydrogen/deuterium in metals

The diffusion of hydrogen and deuterium in metals has been extensively studied by conventional neutron scattering and other techniques. Correlation effects in diffusion can be studied by observing the coherent quasielastic scattering of deuterium; spin analysis is required to separate the coherent and incoherent scattering. Good Q and energy resolutions are required for diffusional studies near Bragg peaks.

3.2 INELASTIC SCATTERING

Neutron spin echo can be used to study the widths of elementary excitations of energies $\hbar\omega_o$. The resolutions obtained for non-dispersive optical branches are limited only by field inhomogeneities, and the "focussed" echo condition can be relatively easily satisfied. Dispersive excitations satisfy the focussing condition only to first order and experimentally complicated methods such as the use of tilted fields are required to achieve focussing[3,9-12]. It is these second order effects which limit the potential energy resolution to perhaps a factor ten worse than those achievable where the limiting factor is the field inhomogeneity.

(a) Nuclear scattering

Neutron spin echo has been used to extend the study of the lifetime of rotons[27] in superfluid ^{4}He at low temperatures by measuring the width of the roton line at a momentum transfer corresponding to the roton minimum. Measurements have also been made on rotons in dilute mixtures of ^{3}He and ^{4}He where energy widths $\hbar\omega$ of the order of 1 μ eV were observed.

Pynn[11,12] has studied the feasibility of measuring transverse and longitudinal acoustic phonons on a triple axis spin echo

spectrometer. Typical examples were taken as the [110] T_2 phonon and [100] L branch phonon in Nb as measured using a conventional triple axis spectrometer by Shapiro et al.[28].

Several other inelastic problems utilising nuclear scattering have been suggested. Lovesey[29] has proposed measuring long wavelength density fluctuations in super-cooled liquids. Coherent inelastic scattering can be used to measure the spectrum of spontaneous density fluctuations. The long wavelength density fluctuations can be described by thermodynamic derivatives and transport coefficients. Low momentum transfers, hQ, and good energy resolution are required. Lovesey and Schofield[30,31] have calculated the coherent scattering function describing the density fluctuations in spherical fluid particles at wavelengths long compared to the interatomic spacing. Models suitable for the liquid droplets, spherical viruses and proteins were described. Inelastic peaks at non-zero frequencies are predicted in the low Q region. The measurement of these excitation widths requires high resolution.

(b) Magnetic scattering

The dynamical properties of ordered nuclear spin systems have been calculated by Word, Heidemann and Richter[32] and the feasibility of measuring nuclear spin waves discussed. Such measurements require high energy resolution at extremely low Q's and are well suited to the NSE method.

Neutrons are a unique tool for measuring crystal field splittings in metallic alloys and compounds[33]. By combining polarisation analysis with the improved energy resolution provided by spin echo, this should allow peak assignments to be verified[34].

4. SPECIFICATION FOR A QUASIELASTIC SCATTERING INSTRUMENT

Table 1 summarises the quasielastic scattering programs currently being studied using neutron spin echo. These include macromolecular diffusion, diffusion in liquid crystals and superionics, spin

relaxation, phase transitions and the diffusion of hydrogen in metals.

With the exception of the measurements of diffusion in superionics and of hydrogen in metals all these experiments could be performed on a spectrometer with the following specification:

(i) Energy resolution, $\hbar\omega \sim 0.01$ to $10\ \mu$eV
(ii) Wavevector transfer range, $Q \sim 0.02$ to $0.4\ \text{Å}^{-1}$
(iii) Wavevector transfer resolution, $\Delta Q \sim 0.005$ to $0.025\ \text{Å}^{-1}$.

For the SNS instrument it is proposed to aim for $\Delta Q/Q \sim 5\%$. This Q resolution is ~ 4 times better than that most frequently used on the IN11 spectrometer where most experiments use $\Delta Q/Q$ ranging from 18% to 35%.

To utilise the main advantages of the pulsed source we require both a large wavelength band, $\Delta\lambda$, and to cover a large scattering angle range with a multidetector.

The first requirement can be achieved by phasing the $\pi/2$ and π coils of the spin echo spectrometer with the SNS pulse; details will be given in section 4(g). Good momentum transfer ($\hbar Q$) resolution is possible as the time-of-flight measurement gives a flight time uncertainly $\delta T/T < 0.5\%$ and $\Delta Q/Q$ is effectively determined by $\Delta\theta/\theta$ even at large scattering angles 2θ.

The maximum wavelength band $\Delta\lambda$ that can be used is limited by the band pass of the polariser and analyser systems and by frame overlap. Due to the possible interference from magnetic material from neighbouring instruments and the instrument beam shutters we have estimated that the critical magnetic precession field regions of the spectrometer must extend out to $\sim$ 15 to 20 metres from the source.

The use of a large angle detector bank dictates that a solenoidal field geometry similar to that on IN11 cannot be used. A vertical field geometry has been proposed, and it will be shown that it is

possible to achieve field homogeneities consistent with the $\hbar\omega$ resolutions specified above with such magnet geometries.

The following detailed design aspects of a pulsed source time-of-flight quasielastic instrument will now be described:

(a) Q range and detector bank,
(b) Flux and wavelength band, $\Delta\lambda$,
(c) Detector solid angle,
(d) Q resolution, $\Delta Q/Q$,
(e) Magnet design,
(f) Energy resolution, $\hbar\omega$,
(g) Phasing of spin turn coils,
(h) Q, τ range,
(i) Polariser and analyser designs.

(a) Q range and detector bank

The optimum choice of the mean incident wavelength, λ_o, is determined by:

(i) the values of ℓ, H and v_o required to achieve the specified energy resolutions (see section 2),

(ii) the source spectrum, and

(iii) limitations associated with the design of the polariser and analyser systems.

These conditions dictate that the mean incident wavelength on the SNS spin echo instrument should be $\lambda_o \sim 6$ Å, and that the spectrometer should ideally view the cold moderator.

We propose to use a static detector array with scattering angles 2θ ranging from 1^o to 21^o. This gives $Q_{min} = 0.018\ \text{Å}^{-1}$ and $Q_{max} = 0.38\ \text{Å}^{-1}$ at $\lambda_o = 6$ Å.

It will be shown in section 4(b) that a wavelength band $\Delta\lambda \sim 3$ Å can be accommodated on the instrument; this means that the effective Q range is extended to $Q_{min} = 0.015$ Å^{-1} and $Q_{max} = 0.51$ Å^{-1}.

(b) Flux and wavelength band $\Delta\lambda$

The most suitable SNS beam hole for a spin-echo instrument is N4; this views the cold moderator and is situated between the low Q and constant Q spectrometers as shown in Figure 2. In order to avoid any magnetic interference from the iron in these neighbouring instruments and the beam shutters, we have placed the polariser at 17 metres from the moderator. If we then assume that the instrument is $\sim$ 6 metres long, then the total neutron flight path to the detector is $\sim$ 23 metres.

In order to avoid frame overlap whilst using each SNS pulse we require,

$$\Delta\lambda \leq 10^6/f.L.\ 252.82 \qquad (4.1)$$

where $\Delta\lambda$ is the maximum wavelength band in Å, f = 50 Hz is the pulse repetition frequency for the SNS and L is the total flight path in metres.

This gives $\Delta\lambda = (79.11/L)$ Å and therefore

$$\Delta\lambda_{max} \sim 3.44 \text{ Å}.$$

By designing the spectrometer to operate at a mean wavelength $\lambda_o = 6$ Å, this gives a useable wavelength band between 4.5 Å and 7.5 Å.

In order to calculate the flux at the sample we shall assume that a straight nickel neutron guide can be placed between the moderator and the start of the spectrometer. To calculate the guide transmittance we assume that the guide and moderator are fully matched for illumination as shown in Figure 3. For a 10 cm square moderator and a guide starting at 2 metres from the moderator, the

matched condition for $\lambda_{max} = 7.5$ Å gives a guide width of 4.8 cm.

If we assume that the fractional losses in the guide are due to surface irregularities then the loss can be expressed as[33]

$$f_L = \frac{L_g \beta}{2}\left[\frac{1}{a} + \frac{1}{b}\right] \qquad (4.2)$$

where,

L_g – guide length,
a,b – cross-sectional dimensions of the guide,
β – surface waviness

then for $\beta \sim 10^{-4}$ radians, $L_g = 15$ m and a=b=4.8 cm, f_L is of the order 3%.

Assuming that the differential neutron flux at the moderator surface is equivalent to the differential neutron flux at the guide entrance when fully illuminated[36], the flux at the guide exit I_g is then given by

$$I_g = \phi_m\, \Omega_t\, (1 - f_L)\ n\ eV^{-1}\ sec^{-1}$$

where,

ϕ_m – differential neutron flux at the moderator surface
Ω_t – guide solid angle of acceptance
and Ω_t – $4\gamma_c^2 = 4\,(0.00173\,\lambda)^2$ for nickel guides.

For the cold (20K) moderator in the 1/E region on the SNS we can write[37]

$$I_g = 4.4 \times 10^{12} \times (0.97) \times 4(0.00173)^2 \times 0.081787 \int_{E_1}^{E_2} \frac{\Delta E}{E^2} \cdot \frac{1}{(10)^2}$$

$$n.cm^{-2}\ sec^{-1}$$

$$= 4.04 \times 10^4 \left[1/E\right]_{E_1}^{E_2}\ n.cm^{-2}\ sec^{-1} \qquad (4.4)$$

and for a wavelength band between 4.5 Å and 7.5 Å we obtain

$$I_g = 1.78 \times 10^7 \text{ n cm}^{-2} \text{ sec}^{-1}$$

If we further assume a polariser transmission of 0.4[38] and a beam divergence loss of 30% in the polariser to sample distance of 2 metres then the calculated flux at the sample position is

$$I_s \sim 2.14 \times 10^6 \text{ n cm}^{-2} \text{ sec}^{-1}$$

This should be compared with a flux at the sample position for IN11 at $\lambda_o = 6$ Å ± 10% of 4.0×10^6 n cm^{-2} sec^{-1}[39]. Note that we have ignored any attenuation effects due to air scattering and have assumed that all flight paths are evacuated.

(c) Detector solid angle

We propose using a 20° 2θ detector array, a sample to detector distance of 3 metres and a detector height of 10 cm. This gives a detector solid angle of the order of 10^{-2} sterad. This compares with the following detector solid angles at other existing or proposed high resolution inelastic spectrometers:

IN11 - the spin echo spectrometer at ILL, 10^{-4} sterad.
IN10 - the ILL backscattering quasielastic spectrometer, 0.4 sterad.
'IRIS - The currently approved SNS quasielastic spectrometer, 0.8 sterad.

The gain factor in solid angle over IN11 is ∿ 100. By taking into account the difference in incident flux the resultant increase in counting rate for the SNS instrument is of the order of 50.

It should be noted that the IN10 and 'IRIS instruments are optimised for incoherent scattering where the neutrons are scattered more or less isotropically into 4π steradians. The complete solid angle available on the SNS instrument may not necessarily be utilised for small angle coherent scattering where the scattering is strongly peaked in the forward direction.

(d) Q resolution, ΔQ/Q

For a time-of-flight diffraction measurement the Q resolution, ΔQ/Q, is given by[40]:

$$(\Delta Q/Q) = [(\Delta\theta \cot\theta)^2 + (\Delta T/T)^2 + \{\Delta(L_o+L_1)/(L_o+L_1)\}^2]^{\frac{1}{2}} \qquad (4.5)$$

where 2θ is the scattering angle, T is the total time-of-flight and L_o, L_1 are the incident and scattered flight paths.

The time-of-flight uncertainty arises from two sources: the moderation width Δt_{mod} at the source and the detector channel width Δt_{det}. For the wavelength band proposed $\Delta t_{mod} \sim$ 100 μsec[41] and if we select detector channel widths ∿ 20 μsec we obtain $\Delta T/T \sim 0.5\%$, which is much greater than the flight path uncertainty. For the proposed instrument the Q resolution is effectively determined by the $\Delta\theta\cot\theta$ term, even at the largest scattering angles.

The experiments listed in Table 1 show that ΔQ values ∿ 0.005 to 0.025 Å^{-1} (ΔQ/Q ∿ 5%) will in general be required. Many of these experiments have in fact been carried out on IN11 with ΔQ/Q ∿ 20% over the Q range 0.02 to 0.2 Å^{-1}. For diffusive processes the averaging of the scattering law over a wide Q resolution is justifiable. It is however advantageous to improve the Q resolution to the values suggested in Table 1, where possible.

We shall now consider the beam divergences in the proposed quasi-elastic instrument (see Figure 4). If α_1, α_2 are the half maximum divergence angles in the incident and scattered arms, then the optimum geometry requires $\alpha_1 \sim \alpha_2$, and $\Delta\theta_{eff}$ is given by:

$$\Delta\theta_{eff} = (\alpha_1^2 + \alpha_2^2)^{\frac{1}{2}} \qquad (4.6)$$

The suggested polariser and analyser systems have multichannel Soller type geometries, and are described in more detail in section 4(i). The effective divergence is then determined by, (i) the analyser and polariser channel widths, (ii) the sample size, and

(iii) the polariser to sample and sample to analyser distances.

If we assume that the polariser to sample distance L_1 and the sample to analyser distance L_2 are $\sim$ 2 metres, p and a are the polariser and analyser channel widths, and s is the sample size, then typical values of $\Delta\theta_{eff}$ for different geometries are shown below:

(i) $p = a = s = 1$ cm; $\alpha_1 = \alpha_2 = 0.29^o$; $\Delta\theta_{eff} = 0.41^o$

(ii) $p = a = 0.5$ cm, $s = 1$ cm; $\alpha_1 = \alpha_2 = 0.21^o$; $\Delta\theta_{eff} = 0.30^o$

(iii) $p = a = 1$ cm, $s = 3$ cm; $\alpha_1 = \alpha_2 = 0.55^o$; $\Delta\theta_{eff} = 0.78^o$

The Q resolutions $\Delta Q/Q$ calculated for these cases are shown in Figure 5. The Q resolution normally obtained on IN11 is included; the improved Q resolution of the time-of-flight instrument over most of the Q range is clearly evident. It is possible to improve the Q resolution on IN11 by using a graphite analyser, but only at the expense of a great loss in flux.

(e) Magnet design

Spin echo measures a polarisation which is proportional to the cosine of the accumulated phase angle so for an ideal system we have (see equation (2.1)):

$$\langle P_y \rangle \alpha \cos(\Omega_o - \Omega_1) \alpha \cos\left(\frac{\gamma_L H_o \ell_o}{v_o} - \frac{\gamma_L H_1 \ell_1}{v_1}\right) \quad (4.7)$$

In a real system there are field integral inhomogeneities which give an effective additional phase shift term ϕ:

$$\langle P_y \rangle_m \quad \alpha \quad \cos\left(\frac{\gamma_L H_o \ell_o}{v_o} - \frac{\gamma_L H_1 \ell_1}{v_1} - \phi\right) \quad (4.8)$$

Hayter[7] has shown that the measured polarisation $\langle P_y \rangle_m$ can be approximated by:

$$\langle P_y \rangle_m = \mathcal{H}\ell \langle P_y \rangle \quad (4.9)$$

where $\mathcal{H}$ is the Fourier transform of the field inhomogeneity distribution.

In practice it has been found that the precession fields must be designed such that $\phi_{max} < 8$ rad otherwise the precessing polarisation is destroyed[2].

The field integral inhomogeneity is also important in determining the maximum field H_{max} utilisable in a spin echo instrument, ie it effectively determines the limiting resolution. This limiting resolution may be expressed as:

$$\varepsilon = \Delta \int H d\ell / \int H d\ell \quad (4.10a)$$

$$= \phi/\Omega \quad (4.10b)$$

$$= \left(\frac{21.59\phi}{H\ell\lambda}\right) = \left(\frac{21.59\ \phi_{max}}{H_{max}\ell\lambda}\right) \quad (4.10c)$$

Equation (4.10c) shows that for given ℓ and λ the additional phase shift ϕ increases with the precession field H but only up to the limiting field H_{max} corresponding to $\phi_{max} \sim 8$ rad, at which point the spin echo polarisation signal is destroyed. For the solenoidal precession fields used on the IN11 instrument the field integral inhomogeneity $\varepsilon \sim 0.0001$[2]. We now demonstrate that comparable ε values can be obtained for the vertical field geometries required in the SNS spin echo instrument.

Pynn[12] has shown that for "racetrack" type windings as illustrated in Figure 6 the maximum line integral inhomogeneities (along the Y-axis in the figure) are given by:

$$\varepsilon_{vert} = cy^2/g(L' + 1.4g) \quad (4.11)$$

where c is a constant $\sim$ 0.4 to 0.7 which depends on $(\partial Hh/\partial Z)$ at y=0, L' is the magnet length and g is the half gap of the magnet. $(L' + 1.4g) = \ell$ represents an effective precession length. Pynn[12] recommends that a minimum c value $\sim$ 0.42 should be attainable and this is the value we have used in our calculations. We present

three possible designs for the SNS instrument precession fields:

(A) g = 25 cm, L' = 100 cm, y = 1.5 cm (this accommodates a 3 cm sample height), $\varepsilon = 0.00028$, $H_{max} \sim 760$ Oe for $\lambda \sim 6$ Å.

(B) g = 35 cm, L' = 100 cm, y = 1.5 cm, $\varepsilon = 0.00018$, $H_{max} \sim 1070$ Oe for $\lambda \sim 6$ Å.

(C) g = 25 cm, L' = 100 cm, y = 1.0 cm, $\varepsilon = 0.000124$, $H_{max} \sim 1230$ Oe for $\lambda \sim 6$ Å.

These magnet designs are considered to be relatively easy to produce at reasonable cost. Shimming and careful optimisation of the design would be required to achieve the stated ε values. ε may be further reduced by the addition of correction coils; this has already been done successfully on the IN11 spectrometer[2,23]. The multiple correction coil being designed at the Rutherford Laboratory by J Coupland for the Oxford Spectrometer Magnet[42] may have interesting possibilities. Hayter and Pynn[43] are currently considering the problem of applying corrections to vertical field geometry precession regions, and investigating the possibility of alternative field configurations to allow large angle detector banks. More detailed magnet design work will be a vital requirement in developing a viable instrument for the SNS.

(f) Energy resolution, $\hbar\omega$

In the calculation of the energy resolution, $\hbar\omega$, we assume that for a Quasielastic Scattering Law $S(Q,\omega)$ which is a Lorentzian, an intermediate scattering law of the following form is measured:

$$p = p_{max}\, e^{-\gamma t} \qquad (4.12)$$

where

$$t = \hbar\Omega_o/2E_o$$

For $p = (1/e)P_{max}$, then $\gamma = 2E_o/\Omega_o\hbar$; where $\hbar\gamma$ is the half

width half maximum of the Lorentzian.

Further it is assumed that the energy resolution is determined by the field inhomogeneities of the precession fields and that the maximum number of precessions Ω_o is determined by equation (4.10c).

For magnet design (C) in section 4(e), $\varepsilon = 0.000124$, and for E_o = 2.27 meV ie $\lambda_o = 6$ Å then $\hbar\gamma \sim 70$ neV.

It appears therefore that the required energy resolutions (see $\hbar\omega$ in Table 1) can be achieved using a vertical field geometry.

(g) Phasing of the spin turn coils

The $\pi/2$ and π spin turn coils have a wavelength dependent action[5,6]; for a large wavelength band $\Delta\lambda$ serious degradations of the echo ratio and hence the signal to noise ratio can occur. On the pulsed source the currents in the spin turn coils and spin flipper can in principle be phased with the pulse and their wavelength dependent efficiencies can either be eliminated or at least minimised.

We present a representative calculation to show that the currents in the spectrometer spin turn coils can be phased with the machine pulse. A typical spin turn coil of the type that can be used on the SNS instrument is shown in Figure 7a.

The coil magnetic field, H_c, can be approximated by

$$H_c \sim \mu_o Ni/L \qquad (4.13)$$

where N is the number of turns in the coil, i is the coil current and L is the length of the coil.

N is typically of the order of 100-150 turns. Following the treatment given for a π-turn coil in reference 5 we have:

β (see Figure 7b) > 0 (4.14)

$H_c = \Gamma_o H_o$, where H_o is the guide field (4.15)

$\Gamma_o = 1/\sin\beta$ (4.16)

$H_c(\text{Oe}) = 67.824/d_o\lambda_o$, (4.17)

where d_o is the coil thickness in cm and λ_o is the neutron wavelength (in Å) at which the coil is perfectly tuned.

For fixed $\beta = 10^o$ we have

(i) At $\lambda = 4$ Å : $H_c = 28.3$ Oe, $H_o = 4.9$ Oe, i $\sim$ 2.25 amps

(ii) At $\lambda = 8$ Å : $H_c = 14.13$ Oe, $H_o = 2.45$ Oe, i $\sim$ 1.12 amps

It is relatively straightforward to change the coil current i to follow the times at which neutrons of different velocities reach the coil: the optimum coil current is, as expected, inversely proportional to the neutron wavelength.

It is also necessary to provide a correction field to adjust for the optimum H_o. This can be produced by a simple Helmholtz pair. We present a typical calculation for the above case where a field compensation $\sim$ 2.5 Oe is required for a wavelength band between 4 Å and 8 Å.

The field from a Helmholtz pair is given by

$$H_{hp} = (0.8)^{3/2} N\, i/a \qquad (4.18)$$

where N is the number of turns in each coil, i the coil currents and 'a' the coil radii. For a = 15 cm, N = 20 we require i $\sim$ 2 amps to provide a compensating field $\sim$ 2.5 Oe. In the case of the SNS spin echo instrument the time required for this $\Delta\lambda$ band to cross the coil is $\sim$ 20 msec, ie a ramping rate $\sim$ 1 amp in 10 msec is required; this is easily achievable.

(h) <u>(Q,τ) range</u>

If we define τ as the Fourier time constant then equation (2.4) for

quasielastic scattering gives

$$\tau = 11.53\, H\ell/v^3 \qquad (4.19)$$

where H is the precession field in Oe, v is the neutron velocity in cm sec^{-1}, and $\ell(= \ell_o = \ell_1)$ are the lengths of the precessional fields in cm.

Further, for the time-of-flight instrument (see equation (2.10))

$$Q = 2\,mv\sin\theta/h = 3.1764 \times 10^{-5}\, v\sin\theta \qquad (4.20)$$

Some typical (Q, τ) scans for ℓ = 150 cm and H ranging from 50 to 900 Oe are shown in Figure 8, for 3 detector angles, 1^o, 10^o and 21^o. A total τ range of 10^{-8} to 5.0×10^{-10} seconds is covered. This is almost identical to the IN11 spectrometer τ range of $\tau = 1.19 \times 10^{-8}$ to 4.8×10^{-10} sec.

(i) <u>Polariser and Analyser design</u>

<u>Polariser</u>

We propose that the polariser can be of the form of a simple straight Soller since the instrument geometry means that the beam is well collimated before and after the polariser. A description of the characteristics of a single channel Soller has been given by Mezei and Schaerpf[38]. The polarisation and reflectivity profiles of the Soller with supermirror surfaces as a function of (θ/λ) are shown in Figure 9, where $\theta_{max} \sim 0.23^o/$Å and $\theta_{min} \sim 0.02^o/$Å (non-reflecting substrate) and $0.06^o/$Å (glass substrate). The criteria used in designing the single channel Soller are illustrated in Figure 10a, with

$$S/L_2 = A_{max} - A_{min} \qquad (4.21)$$

$$A_{max} = 2D/L_M \qquad (4.22)$$

$$A_{min} = [2D/L_M - S/L_2] \qquad (4.23)$$

It is convenient to discuss the properties of the polariser in terms of the variation of its polarisation transmittance product, P * T, at the following wavelengths:

$$\lambda_1 = A_{min}/\theta_{max} \quad (4.24)$$

$$\lambda_2 = A_{max}/\theta_{max} \quad (4.25)$$

$$\lambda_3 = A_{min}/\theta_{min} \quad (4.26)$$

$$\lambda_4 = A_{max}/\theta_{min} \quad (4.27)$$

The wavelength dependence of P * T for the single channel polariser is shown in Figure 11. Some typical designs, where the P * T product has been optimised over the wavelength range of interest to the spin echo spectrometer are shown in Table 3. The 110 cm long Soller design is close to the optimum for this instrument.

In order to cover conventional sample sizes we propose using a focussing system as shown in Figure 10b. Five channels, each 1 cm wide, are sufficient for a 3 cm sample. The parameters given in Table 3 show that over the wavelength range of interest (4.5 to 7.5 Å) the design is relatively straightforward.

It is not at present technically feasible to build a curved Soller polariser to cover the required wavelength range.

Analyser

A possible analyser system for the spectrometer is shown in Figure 12a where the analyser consists of a multichannel V-shaped Soller and each analyser channel is viewed by a single detector element. The important design parameters for a single channel of the analyser are shown in Figure 12b where,

$$A_{max} - A_{min} = S/L_{SA} \quad (4.28)$$

$$A_{max} = 2d/L_M \quad (4.29)$$

$$\theta_M = [A_{max} - A_{min}]/2 \quad (4.30)$$

$$L_{sD} = L_{sA} + L_{M/2} + L_S \quad (4.31)$$

A possible set of values for the analyser parameters are listed in Table 4. This design should be relatively easy to construct.

(j) Summary

The proposed quasielastic scattering instrument is shown schematically in Figure 13. A comparison of the important parameters of the proposed quasielastic instrument with those of IN11, IN10 and 'IRIS is presented in Table 5. A summary of the types of measurement appropriate for the respective high resolution instruments is given in Table 6.

Detailed design work is required particularly on the precession fields though the preliminary work suggests that the required field integral homogeneities should be attainable. A simple disc chopper is required to select the spectrometer wavelength band; its design is very straightforward.

The resolution that can eventually be attained on the instrument will be very dependent on the degree of magnetic interference from neighbouring metallic structures. Unfortunately this is very difficult to quantify, however we do urge, where possible, that any future design of instrumentation in the vicinity of the N4 beam port should attempt to take this into account.

In conclusion, the time-of-flight neutron spin echo spectrometer for high resolution quasielastic scattering studies has been shown to have a comparable performance with existing high resolution spectrometers, but it has the additional advantage of having a superior Q resolution.

5 SPECIFICATION FOR AN INELASTIC SCATTERING INSTRUMENT

We shall now consider the design of a time-of-flight spin echo spectrometer that can be used to measure the widths of elementary excitations. The basic instrument is a chopper spectrometer as suggested by Mezei[15]. Although some of the features of the design are similar to those of the quasielastic spectrometer there are several important differences.

The "focussed" echo condition can be satisfied for quasielastic and non-dispersive inelastic excitations such that the energy resolution is limited only by the precession magnetic field inhomogeneities, and energy resolutions of the order of 10^{-7} to 10^{-8} eV have been achieved[2]. For inelastic excitations which are dispersive, the energy resolution is limited to about 10^{-5} to 10^{-6} eV due to second order effects of the "focussing" condition[3,9-12]. Furthermore the "focussed" condition can only be satisfied to first order if a "tilted" precession magnet geometry[3,11,12] is employed.

The types of inelastic scattering studies envisaged are summarised in Table 2, and discussed in more detail in Section 3. Some of these measurements such as density fluctuations in supercooled liquids, compression modes in molecular aggregates, and the study of nuclear spin waves are highly speculative. The phonon studies in superfluid He and Niobium are typical examples of a wide range of phonon studies. The problem of detecting nuclear spin waves[32] and the need for very low scattering vectors suggests that such experiments would be beyond the capability of the first generation time-of-flight spin echo spectrometers.

The quasielastic time-of-flight spectrometer can be used to study non-dispersive excitations, however, we would recommend, that because of the incompatibilities of the precession field requirements, there should ideally be a separate instrument dedicated for inelastic experiments. In view of the second order effects of the focussing condition we have designed the precession field magnets for the inelastic instrument to give an energy resolution in the

range 1 to 10 μeV. The lower number of precessions required means that shorter magnets may be used; the total instrument length need be no longer than ∿ 4 metres.

The Q range required (0.02 to 0.2 Å^{-1} and 0.4 to 2.0 Å^{-1}) suggests the need to use two detector banks; a 50° bank for the Q range associated with normal phonon studies, and a low angle array for studying density fluctuations in supercooled fluids and the collective modes in molecular aggregates. The designs for the spin turn coils, the polariser and the analyser are similar to those presented for the quasielastic spectrometer, and will not be considered further.

The following aspects will be considered in more detail:

(a) Flux and wavelength band $\Delta\lambda$
(b) Q range and detector array
(c) Energy resolution and magnetic field design
(d) Maximum energy transfer, $\hbar\omega$
(e) Chopper

(a) Flux and wavelength band

The factors affecting the choice of the mean incident wavelength λ_o are similar to those presented for the quasi-elastic instrument in Section 4(a). The choice of two possible mean incident wavelengths, namely $\lambda_o \sim 4$ Å and 6 Å, will be considered for the inelastic instrument and we shall assume as for the quasielastic instrument that the inelastic instrument will view the 20K cold moderator and start at ∿ 17 metres from the moderator so as to minimise the magnetic interference from adjacent metallic structures.

For a total instrument length of 4 metres the wavelength band that can be used without frame overlap becomes

$$\Delta\lambda = 79.11/21 = 3.5 \text{ Å}$$

The wavelength limits and corresponding sample fluxes, calculated assuming chopper transmittances $\sim$ 70% are shown below:

Mean Wavelength λ_o	Maximum Wavelength λ_{max}	Minimum Wavelength λ_{min}	Sample Flux n cm^{-2} sec^{-1}
4Å	5.5Å	2.5Å	1.0×10^6
6Å	7.5Å	4.5Å	1.5×10^6

(b) Q range

In order to have the capability to carry out experiments over the Q range discussed in Section 3 we suggest the following possible detector arrangements.

(i) At λ_o = 4 Å:

(A) A 50° detector bank with $2\theta_{min} = 20°$, $2\theta_{max} = 70°$, and $\Delta\lambda$ = 3 Å to give $Q_{min} \sim 0.39$ $Å^{-1}$ and $Q_{max} \sim 2.9$ $Å^{-1}$.

(B) A 4° low Q detector array with $2\theta_{min} = 1°$, $2\theta_{max} = 5°$, and $\Delta\lambda$ = 3 Å, to give $Q_{min} \sim 0.02$ $Å^{-1}$ and $Q_{max} \sim 0.22$ $Å^{-1}$.

(ii) At λ_o = 6 Å:

(A) A 50° detector bank with $2\theta_{min} = 50°$, $2\theta_{max} = 100°$, and $\Delta\lambda$ = 3 Å to give $Q_{min} \sim 0.71$ $Å^{-1}$ and $Q_{max} \sim 2.2$ $Å^{-1}$.

(B) A 4° low Q detector array with $2\theta_{min} = 1°$, $2\theta_{max} = 6°$, and $\Delta\lambda$ = 3 Å to give $Q_{min} = 0.037$ $Å^{-1}$ and $Q_{max} = 0.15$ $Å^{-1}$.

(c) Magnet design and energy resolution

The magnetic field design and the resulting energy resolution follows the arguments presented in Sections 4(e) and 4(f). The following design parameters are considered suitable for a vertical field precession field magnet with "racetrack" type windings:

y = 1.5 cm, L' = 25 cm, g = 10 cm giving ε = 0.0023, H_{max} = 480 Oe (at λ_o = 4 Å) and H_{max} = 320 Oe (at λ_o = 6 Å).

Assuming a Lorentzian lineshape the corresponding energy resolutions are $\hbar\gamma$ = 3 μeV (at λ_o = 4 Å) and $\hbar\gamma$ = 1.3 μeV (at λ_o = 6 Å).

This design means that the energy resolution in the proposed inelastic instrument is limited by field inhomogeneities rather than by second order focussing effects. More detailed calculations will be required before a firm decision can be made on the optimum magnet design. These should include the effects of tilting the precession fields to obtain focussing as suggested by Mezei[9] for a triple axis spin-echo spectrometer.

(d) Limitation in energy transfer ranges $\hbar\omega_o$

For inelastic measurements where the two precession field lengths before and after the scatterer are equal the focussed echo condition for the non-dispersive case (see equation (2.5)) is:

$$(H_o/H_1) \propto (v_o/v_1)^3 \propto (\lambda_1/\lambda_o)^3 \qquad (5.1)$$

and this restricts the maximum energy transfer $\hbar\omega_o$ to which the spectrometer can be tuned. This is essentially because there are practical limits to the magnitude of (H_o/H_1) ie $(H_o/H_1)_{max} \sim 100$, $(H_o/H_1)_{min} \sim 1/100$.

For neutron down-scattering:

$$(H_o/H_1) \sim 10^2 \sim (\lambda_{1max}/\lambda_o)^3 \qquad (5.2)$$

ie $\lambda_{1max} \sim 4.641\ \lambda_o$

This relation gives the following energy transfer limits at incident wavelengths λ_o = 4 Å and 6 Å:

λ_o	E_o(meV)	λ_{1max}	E_{1min} (meV)	$\hbar\omega_{max}$ (meV)
4Å	5.11	18.6Å	0.24	4.87
6Å	2.27	27.9Å	0.11	2.16

For neutron up-scattering:

$$(H_o/H_1) \sim 1/10^2 \sim (\lambda_{1min}/\lambda_o)^3$$

ie $\lambda_{1min} \sim 0.215\ \lambda_o$

The energy transfer limits at λ_o = 4 Å and 6 Å are:

λ_o	E_o(meV)	λ_{1min}	E_{1max}(meV)	$\hbar\omega_{max}$(meV)
4Å	5.11	0.86Å	110.6	105.5
6Å	2.27	1.29Å	49.1	46.8

A further limitation is imposed if the same energy resolutions are required at all energy transfers. This point may be illustrated for the case of a Lorentzian scattering law where the energy resolution may be expressed in terms of the linewidth parameter γ, as discussed in Section 4(f), where

$$\hbar\gamma = \frac{2E_1}{\Omega_1} = \frac{2E_o}{\Omega_o} \qquad (5.4)$$

For down-scattering,

$$\hbar\omega_{max} = E_o - E_{1min} \qquad (5.5)$$

is limited by H_{1min} in the scattered beam. Substituting

$$\Omega_1 = (H_{1min}\ \ell_1\ \lambda_{1max}/21.59)\ \text{rad.} \qquad (5.6)$$

where H is in Oe, ℓ in cm and λ in Å, gives the limiting condition for down-scattering:

$$E_{1min} = (H_{1min}\ \ell_1\ \hbar\gamma/4.77)^{2/3}\ \text{meV} \qquad (5.7)$$

and $\hbar\gamma$ is also expressed in meV.

As a typical example we shall take

$$H_{1min} \sim 10\ \text{Oe};\quad \hbar\gamma \sim 3 \times 10^{-3}\ \text{meV},\quad \ell_1 = 50\ \text{cm},$$

and this gives $\hbar\omega_{max} \sim 4.64$ meV at an incident wavelength $\lambda_o \sim 4$ Å. Note that this is very similar to the $\hbar\omega_{max}$ value calculated ignoring the energy resolution.

A different result is obtained for neutron up-scattering. Here $\hbar\omega_{max}$ is limited by H_{1max} ie

$$E_{1max} = (H_{1max}\ \ell_1\ \hbar\gamma/4.77)^{2/3}\ \text{meV} \qquad (5.8)$$

and using $H_{1max} = 10^3$ Oe, ℓ_1 = 50 cm, $\hbar\gamma = 3 \times 10^{-3}$ meV we obtain $\hbar\omega_{max} \sim 7.8$ meV at an incident wavelength $\lambda_o \sim 6$ Å, which is significantly smaller than in the calculation which ignores the energy resolution.

We conclude that for inelastic NSE experiments with cold neutron beams at resolutions of a few microvolts, the energy transfer ranges $\hbar\omega$ measurable are limited to $\sim$ 10 meV for both neutron up-scattering and down-scattering. The energy transfer values presented in Table 2 for the experiments so far suggested are all within this range.

(e) Chopper

Adding a chopper phased with the SNS pulse before the first

polariser gives a time-of-flight spectrometer combined with spin echo. In the absence of the chopper each time-of-flight channel in the detector collects data over large regions of $S(Q,\omega)$. Spin echo acts as a focus for a given part of the scattering (determined by equation (2.9)) and the rest of the scattered intensity appears as an unpolarised background. If weak inelastic effects are being investigated in the presence of, for example, strong Bragg scattering it will almost certainly be necessary to use a limited incident energy band. This chopper should have a wavelength resolution $\Delta\lambda/\lambda \sim 2$ to 20% at variable λ_0. Either a multi-slot straight velocity selector at a variable angle to the neutron beam or a single disc chopper could be used to provide this function.

(f) Summary

The design of an inelastic NSE scattering spectrometer for the SNS has been outlined. Comparisons with other inelastic NSE spectrometers are not possible since very few measurements of this type have been carried out to date. As with the quasielastic spectrometer, the inelastic spectrometer would provide a unique facility.

ACKNOWLEDGEMENTS

It is a pleasure to acknowledge our helpful discussions with F Mezei, who first suggested combining the time-of-flight and NSE techniques, J B Hayter for his clarification of many of the details of the method, S W Lovesey and C J Carlile for numerous discussions on the areas of application and J Simkin for his advice on magnet design.

TABLES

Table 1: Quasielastic Scattering Experiments ($\hbar\omega_0 = 0$) using NSE

System	$\hbar\omega$	Q range	ΔQ
(a) Macromolecular diffusion			
Micelles[16,17]	10 to 200neV	0.02 to 0.2Å^{-1}	0.005Å^{-1}
Polymers (in solution and melt)[18-20]	10neV to 1μeV	0.05 to 0.15Å^{-1}	0.005Å^{-1}
Haemoglobin[21,22]	10 to 500neV	0.02 to 0.25Å^{-1}	0.005Å^{-1}
Viruses[22,23]	10 to 500neV	0.02 to 0.25Å^{-1}	0.005Å^{-1}
Proteins[23]	10 to 500neV	0.02 to 0.25Å^{-1}	0.005Å^{-1}
(b) Diffusion in liquid crystals and superionics			
Liquid crystals[23]	0.5 to 10μeV	0.1 to 0.4Å^{-1}	0.01Å^{-1}
Superionics (eg $SrCl_2$)[22]	0.8 to 80μeV	1.0 to 2.0Å^{-1}	0.1Å^{-1}
(c) Spin relaxation			
Spin glasses			
(i) Cu-Mn[24]	50neV to 10μeV	0.1 to 0.4Å^{-1}	0.025Å^{-1}
(ii) $Al_2Mn_3Si_3O_{12}$[23]	50neV to 10μeV	0.1 to 0.2Å^{-1}	0.01Å^{-1}
(d) Phase transitions			
Critical dynamics in organic molecules and liquid crystals			
(i) P-terphenyl[23,25]	0.1 to 1μeV	-	0.01Å^{-1}
(ii) Nematic-smectic A phase transition in CBOOA[23]	10neV to 1μeV	0.01 to 0.05Å^{-1}	0.01Å^{-1}
(e) Diffusion of hydrogen/deuterium in metals			
$Pd_{(1-x)}D_x$[26]	0.1 to 0.5μeV	0.5 to 2Å^{-1}	0.05Å^{-1}

Table 2: Inelastic Scattering Experiments ($\hbar\omega_o \neq 0$) using NSE

System	$\hbar\omega_o$	$\hbar\omega$	Q range	ΔQ	Comments
(a) Nuclear Scattering					
Roton lifetime in $^4He^{27}$	0.8meV	1μeV	1.9Å^{-1}	0.02Å^{-1}	non-dispersive
Other phonons in $^4He^{27}$	0.85meV	1μeV	1.7 to 2.4Å^{-1}	0.04Å^{-1}	Dispersive
Niobium [110] T_2	2.38meV	1 to 50μeV	-	-	Dispersive
[100] L[11,12,28]	6.6meV	1 to 50μeV			
Density fluctuations in supercooled liquids[29]	0.2 to 0.5meV	0.1 to 1.0μeV	0.01 to 0.05Å^{-1}	0.005Å^{-1}	-
Compression modes in molecular aggregates[30,31]	0.1 to 0.5meV	1.0 to 10.0μeV	0.02 to 0.1Å^{-1}	0.0025Å^{-1}	-
(b) Magnetic Scattering					
Nuclear Spin Waves[32,33]	0.5 to 4.0μeV	$\lesssim$ 1μeV	10^{-2} to 10^{-3}Å^{-1}	2.5×10^{-3} Å^{-1}	Dispersive
Crystal field splittings[33,34]	0 to 5meV	$\sim$ 10μeV	0.5 to 3.0Å^{-1}	0.05Å^{-1}	-

Table 3: Polariser Design (See Figure 10)

$\alpha_{max} = 0.23^o$

$\alpha_{min} = 0.02^o$

Sample size = 3 cm

Polariser to sample distance = 200 cm

D (cm)	L_M (cm)	A_{max}	A_{min}	λ_1(Å)	λ_2(Å)	λ_3(Å)	λ_4(Å)
1.0	50.0	2.29^o	1.43^o	6.23	9.97	71.6	114.6
1.0	60.0	1.91^o	1.05^o	4.57	8.3	52.5	95.5
1.0	70.0	1.64^o	0.78^o	3.38	7.1	38.9	81.9
1.0	80.0	1.43^o	0.57^o	2.49	6.23	28.65	71.6
1.0	90.0	1.27^o	0.41^o	1.8	5.54	20.69	63.7
1.0	100.0	1.15^o	0.29^o	1.25	4.98	14.23	57.3
1.0	110.0	1.04^o	0.18^o	0.79	4.53	9.12	52.1

Table 4: Analyser Design (See Figures 12a and 12b)

$\alpha_{max} = 0.23^o$

$\alpha_{min} = 0.06^o$

Detector angle = 2.0^o

Sample size = 3.0 cm

Analyser channel width = 1.0 cm

Sample to Analyser distance L_{SA}, = 3 m, L_M = 110 cm,
L_S = 26.32 cm

$A_{max} = 1.042^o$

$A_{min} = 0.47^o$

$\lambda_1 = 2.03$ Å $\lambda_2 = 4.53$ Å $\lambda_3 = 7.81$ Å $\lambda_4 = 17.4$ Å

Angle of mirror 1 with respect to detector angle, straight through position = 0.76^o, 2.76^o

Angle of mirror 2 with respect to mirror 1, straight through position = 0.76^o, 3.14^o

Table 5: Comparison of High Resolution Instruments

Instrument	Flux @ sample in ncm^{-2} sec^{-1}	Detector Solid Angle (sterad)	Energy Resolution (FWHM)
'IRIS	3×10^3	0.8	2.0 μeV
IN10	10^3	0.4	1.0 μeV
IN11	4×10^6	10^{-4}	0.030 μeV
SNS NSE (Quasielastic)	2×10^6	10^{-2}	0.070 μeV

Table 6: Use of High Resolution Instruments for Different Types of Measurement

Type of measurement	'IRIS	IN10	IN11	SNS NSE
Tunnelling, hyperfine splitting	✓	✓	X	X
Spin incoherent scattering	✓	✓	X	X
Single Lineshape analysis	X	X	✓	✓
Strong Q dependence around Q = 0	X	X	X	✓
Q dependence at small θ	X	X	✓	✓

FIGURE CAPTIONS

1) Qualitative (Q,ω) representation of the various types of inelastic scattering processes.

2) SNS beam layout showing the position of the most suitable beam hole (N4) for a spin-echo instrument.

3) Matching condition for a neutron guide between the moderator and the quasielastic spin-echo instrument.

4) Beam divergence criteria which determine the Q resolution of the SNS quasielastic spin-echo instrument.

5) Q resolutions, $\Delta Q/Q$, for various geometries of the quasielastic spin-echo instrument. $\Delta Q/Q$ for the IN11 instrument is also included for comparison.

   □ - IN11 instrument

   ● - $p = a = s = 1$ cm, $L_1 = L_2 = 2$ m

   o - $p = a = 0.5$ cm, $s = 1$ cm, $L_1 = L_2 = 2$ m

   × - $p = a = 1$ cm, $s = 3$ cm, $L_1 = L_2 = 2$ m

6) Vertical Field geometry precession magnet with "racetrack" windings.

7) Schematic representation of a typical spin turn coil. (a) Coil geometry and (b) coil axes. H_o is the guide field, H_c is the spin turn coil field, and H_N is the resultant field inside the coil.

8) (Q,τ) scans for a quasielastic spin-echo instrument. Precession field lengths, $\ell = 150$ cm, scattering angle range, $2\theta = 1^o$, 10^o and 20^o.

   (a) H = 50 Oe.

   (b) H = 450 Oe.

   (c) H = 900 Oe.

9) Reflectivity and Polarisation profiles for a typical polarising "supermirror".

10) (a) Representation of one channel of a Soller polariser.

    (b) Representation of a full focussing Soller polariser system.

11) $P(\lambda)$ *$T(\lambda)$ product for a typical Soller polariser.

12) (a) Representation of a focussing Soller analyser system.

    (b) Representation of one channel of the spin analyser system suggested for the SNS NSE instrument.

13) Schematic diagram of the proposed spin-echo Quasielastic TOF instrument.

REFERENCES

1. F Mezei, Z Physik 255 146 (1972).

2. "Neutron Spin Echo", Ed: F Mezei, Lecture Notes in Physics 128 Springer Verlag (1980).

3. F Mezei, "The Principles of Neutron Spin Echo" in reference 2.

4. J B Hayter, "The Theory of Neutron Spin Echo Spectrometry" in reference 2.

5. J B Hayter, Z Physik B31 117 (1978).

6. J B Hayter and J Penfold, Z Physik B35 199 (1979).

7. J B Hayter, Institut Laue-Langevin Internal Scientific Report, 78HA50 (1978).

8. J B Hayter, in "Neutron Diffraction", Ed: H Dachs, Berlin. Springer Verlag (1978).

9. F Mezei, "Neutron Spin Echo and Polarised Neutrons", in "Neutron Inelastic Scattering", Conf Proc IAEA, Vienna, 1978, p.125.

10. F Mezei, in "Proceedings of the Third International School on Neutron Scattering", Alushta, (Joint Institute of Nuclear Research, Dubna, 156, (1978)).

11. R Pynn, J Phys E 11 1133 (1978).

12. R Pynn, "Neutron Spin Echo and Triple Axis Spectrometers" in reference 2.

13. P A Dagleish, J B Hayter and F Mezei, "The IN11 Neutron Spin Echo Spectrometer" in reference 2.

14. O Scharpf, "The Polarised Neutron Technique of Neutron Spin Echo" in reference 2.

15. F Mezei, Nucl Inst Meth 164 153 (1979).

16. J B Hayter and J Penfold, "Dynamics of Concentrated Micellar Solutions", in reference 2.

17. J B Hayter and J Penfold, accepted for publication in J C S Faraday I.

18. L K Nicholson, J S Higgins and J B Hayter, "Dynamics of Dilute Polymer Solutions", in reference 2.

19. L K Nicholson, J S Higgins and J B Hayter, submitted to Polymer.

20. D Richter, J B Hayter, F Mezei and B Ewan, Phys Rev Lett 41 1484 (1978).

21. Y Alpert, "Tentative Use of NSE in Biological Studies" in reference 2.

22. Institut Laue-Langevin Annual Report (1978) Ed: B Maier.

23. Institut Laue-Langevin Annual Report (1979) Ed: B Maier.

24. F Mezei and A P Murani, J Mag and Mag Mat 14 211 (1979).

25. H Cailleau, A Heidemann and C M E Zeyen, J Phys C 12 L411 (1979).

26. C J Carlile - private communication.

27. F Mezei, Phys Rev Lett 44 1601 (1980).

28. S M Shapiro, G Shirane and J D Axe, Phys Rev B 12 4899 (1975).

29. S W Lovesey, Z Physik B34 323 (1979).

30. S W Lovesey and P Schofield, J Phys C 9 2843 (1976).

31. P Schofield, "Coherent Inelastic Scattering in Inhomogeneous Media", in Neutron Inelastic Scattering, 1977 (IEAE, Vienna 1978) 637.

32. R Word, A Heidemann and D Richter, Z Physik B28 23 (1977).

33. S W Lovesey - private communication.

34. "Crystalline Electric Fields in Metals and Alloys", Ed: A Furrer, Plenum Press (1977).

35. M W Johnson, Rutherford Laboratory Guides Working Party Report, GWP/3/80.

36. C J Carlile, M W Johnson and W G Williams, "Neutron Guides on Pulsed Sources", Rutherford Laboratory Internal Report, RL-79-084 (1979).

37. A D Taylor - private communication.

38. F Mezei and O Schaerpf - unpublished work.

39., F Mezei - private communication.

40. R N Sinclair, D A G Johnson, J C Dore, J H Clarke and A C Wright, Nucl Inst Meth 117 445 (1974).

41. A D Taylor, Rutherford Laboratory Internal Report, TRAM/P2/80 (1980).

42. J Simpkin - private communication.

43. J B Hayter and R Pynn - private communication.

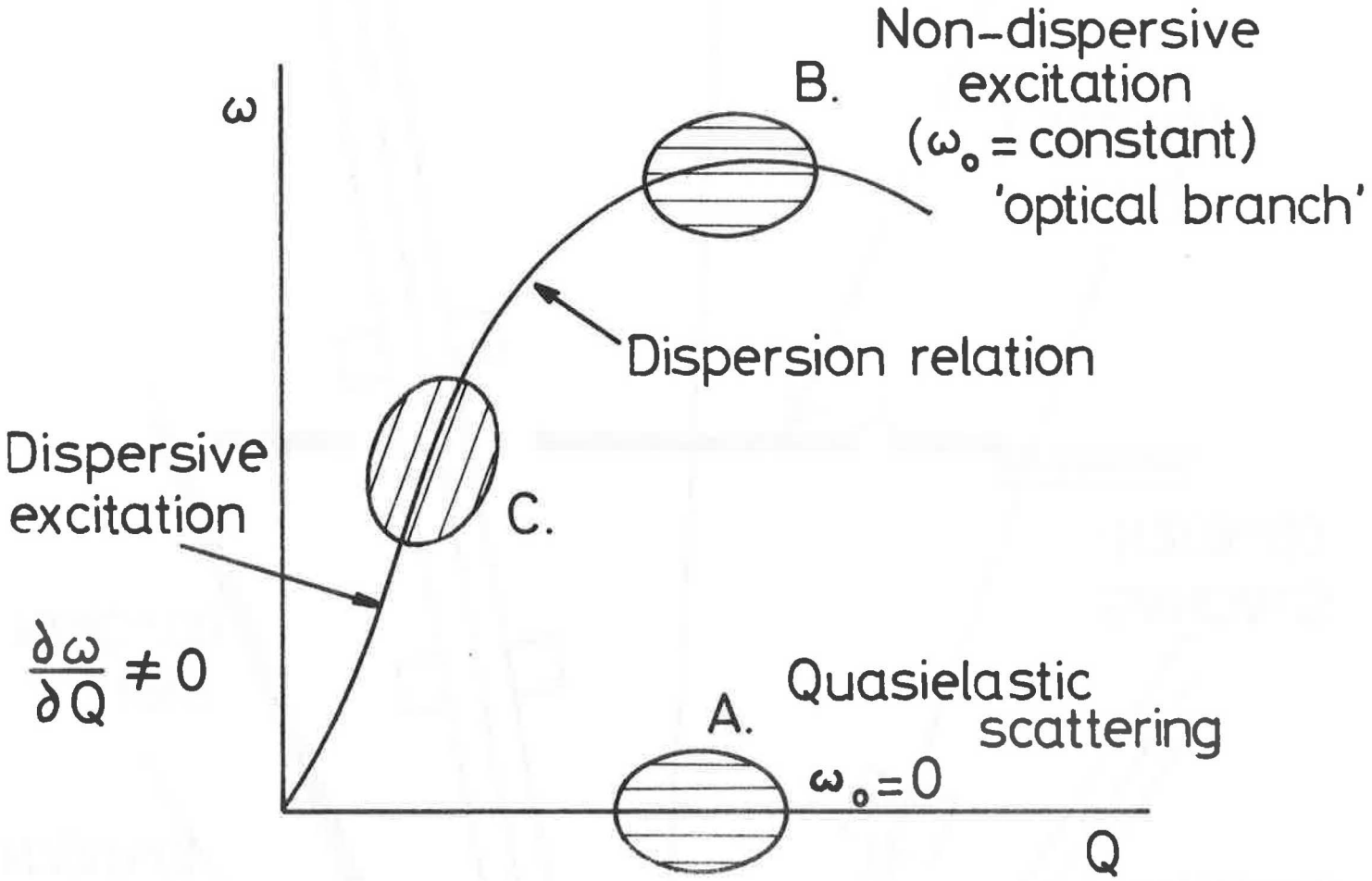
ω
B.
Non-dispersive
excitation
(ω_0 = constant)
'optical branch'
Dispersion relation
Dispersive
excitation
C.
$\frac{\partial \omega}{\partial Q} \neq 0$
A.
Quasielastic
scattering
$\omega_0 = 0$
Q

Figure 1

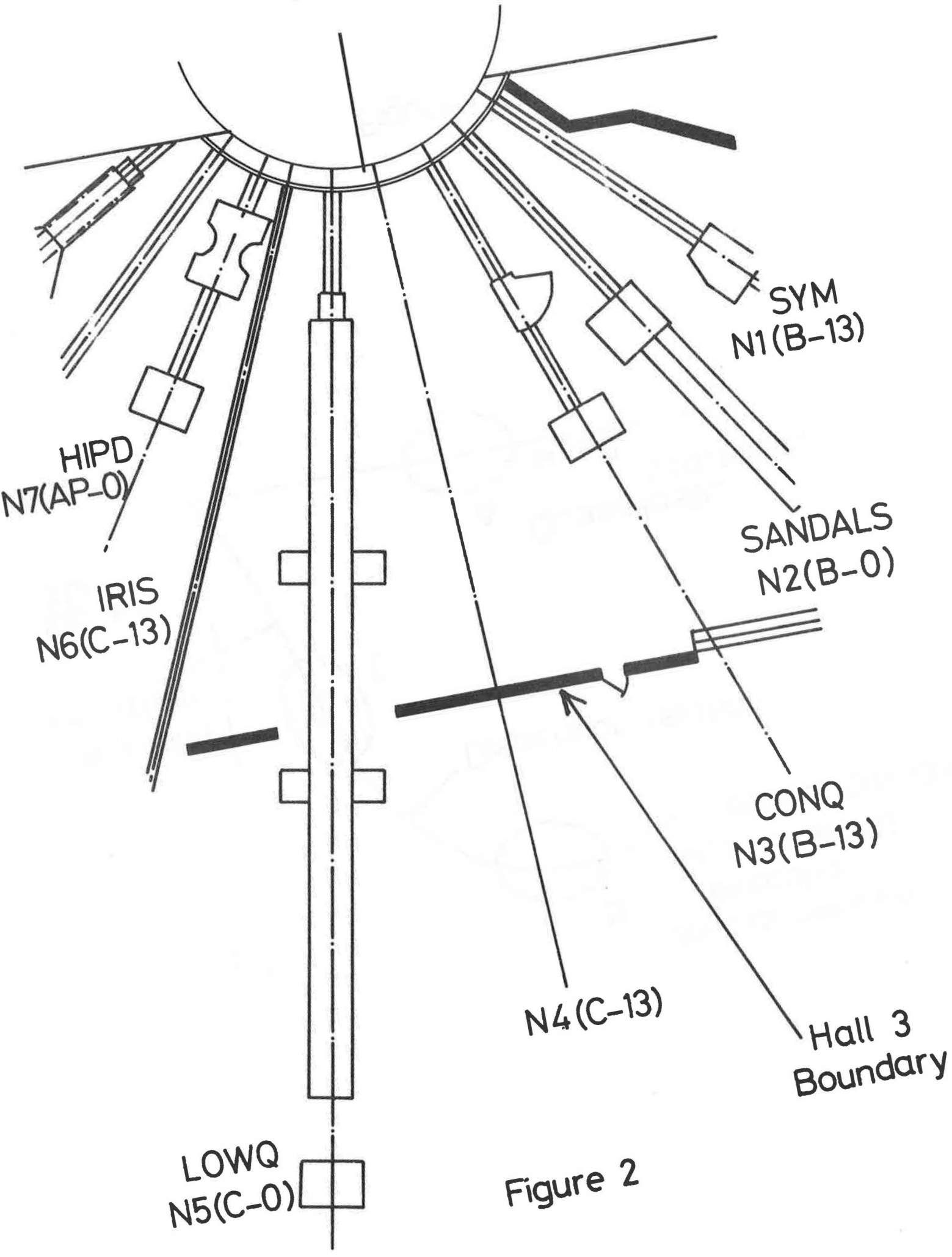
SYM
N1(B-13)
HIPD
N7(AP-0)
SANDALS
N2(B-0)
IRIS
N6(C-13)
CONQ
N3(B-13)
N4(C-13)
Hall 3
Boundary
LOWQ
N5(C-0)

Figure 2

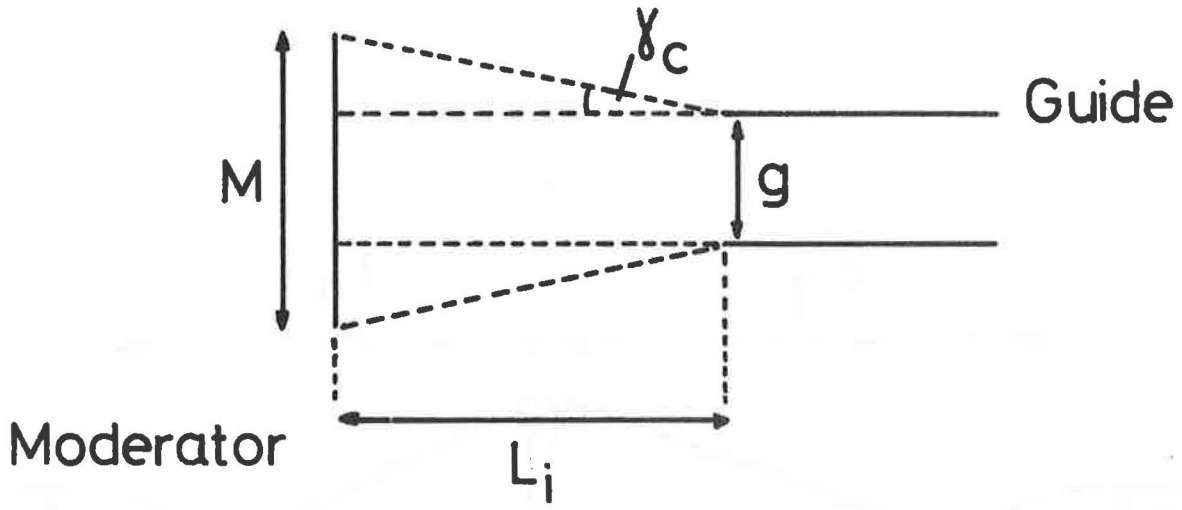

Figure 3

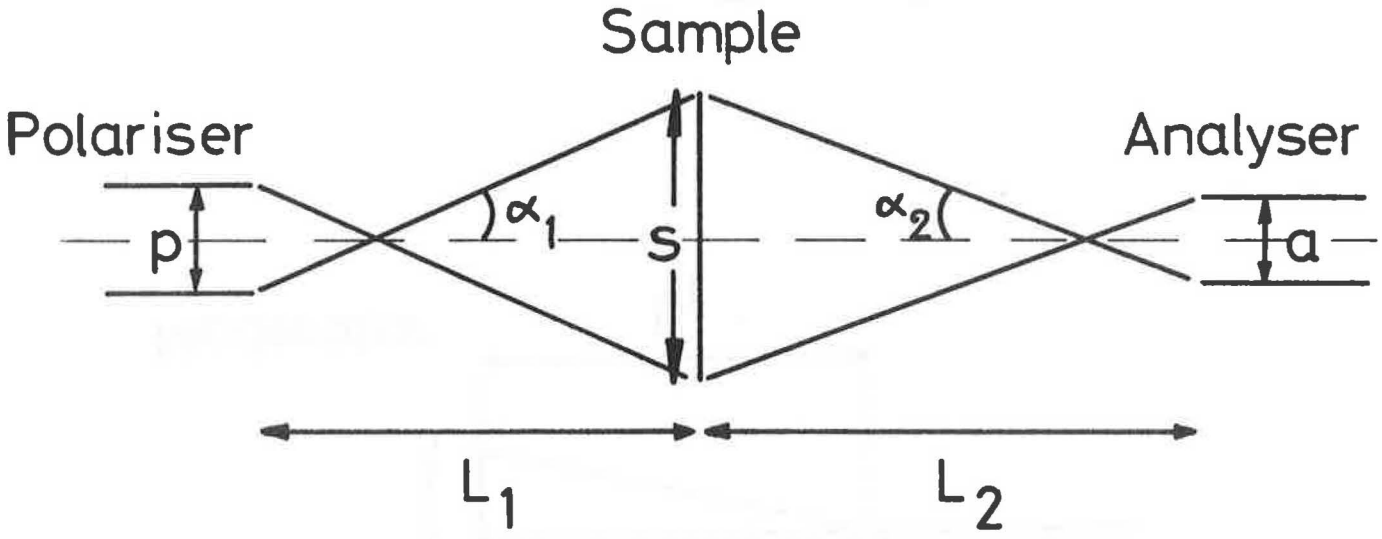

Figure 4

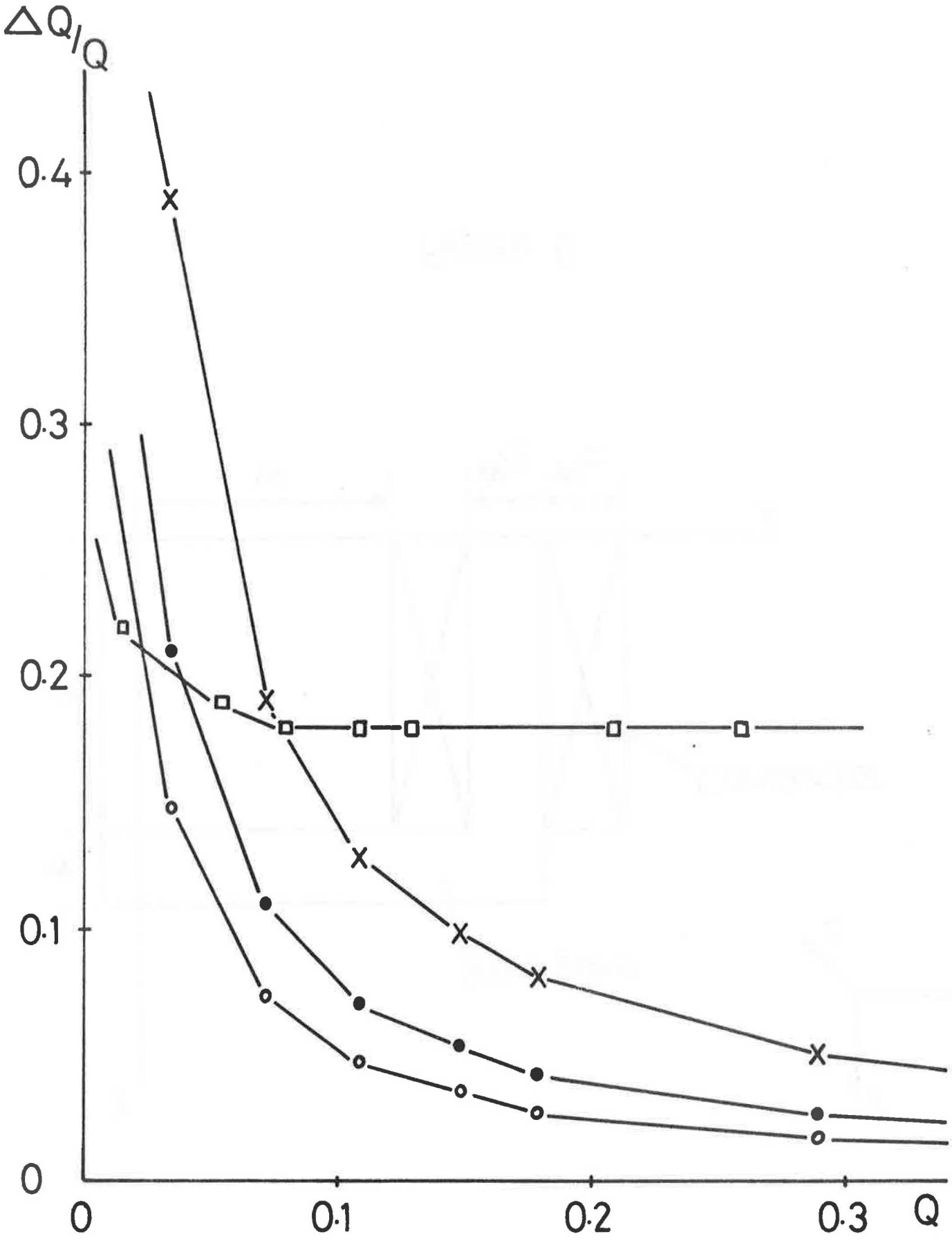

Figure 5

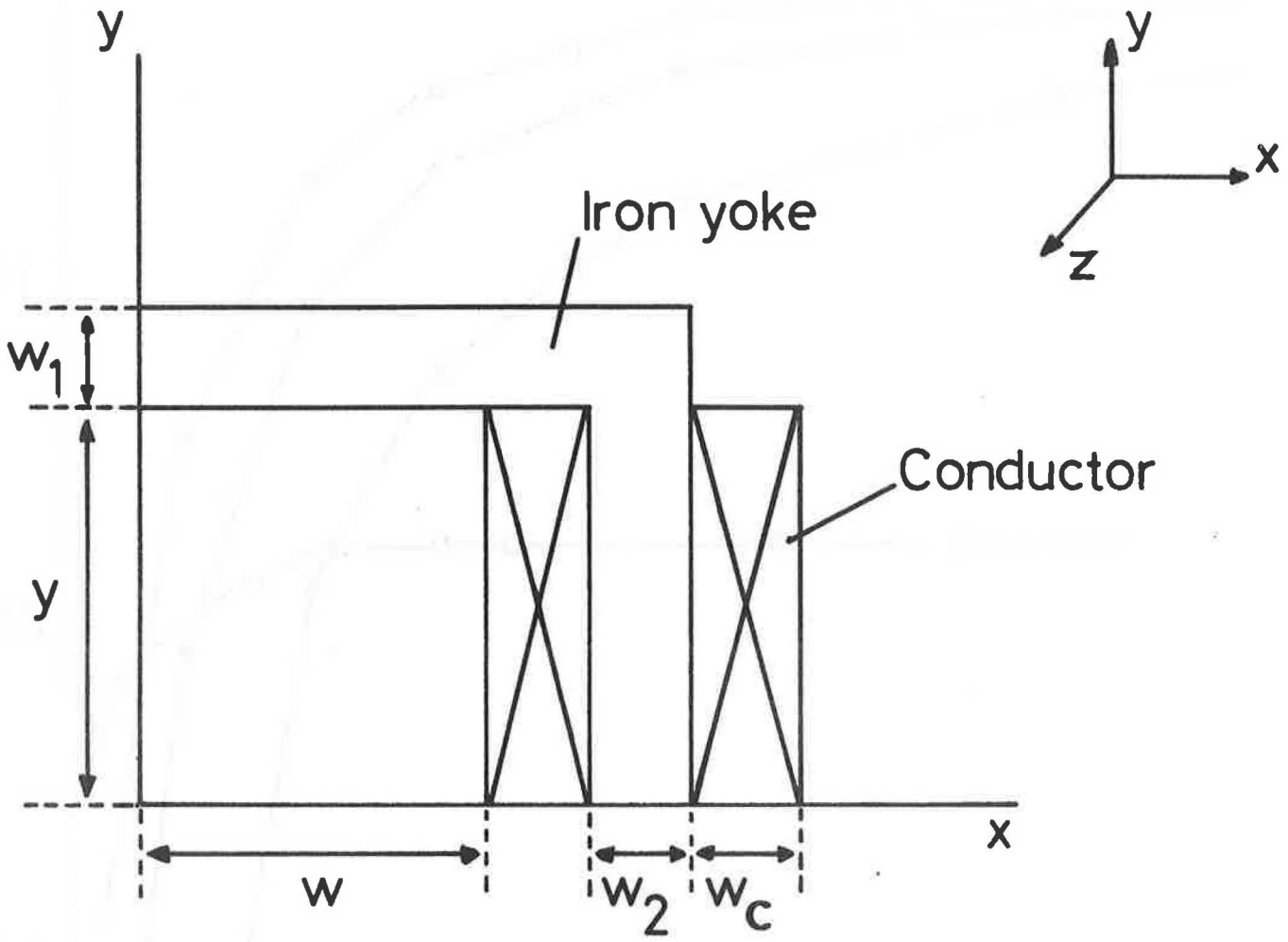

Figure 6

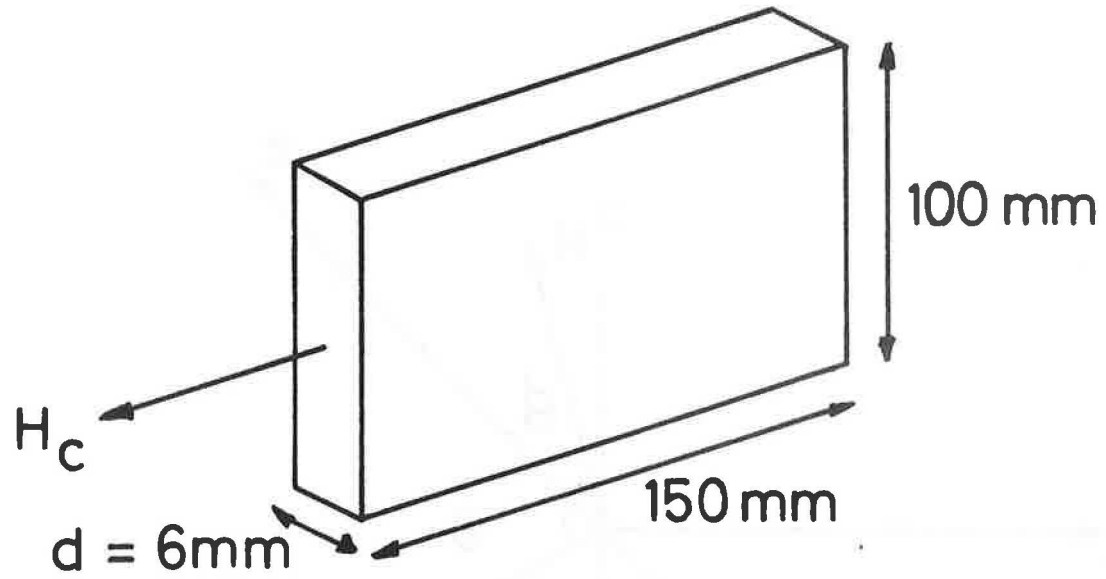

(a)

Figure 7

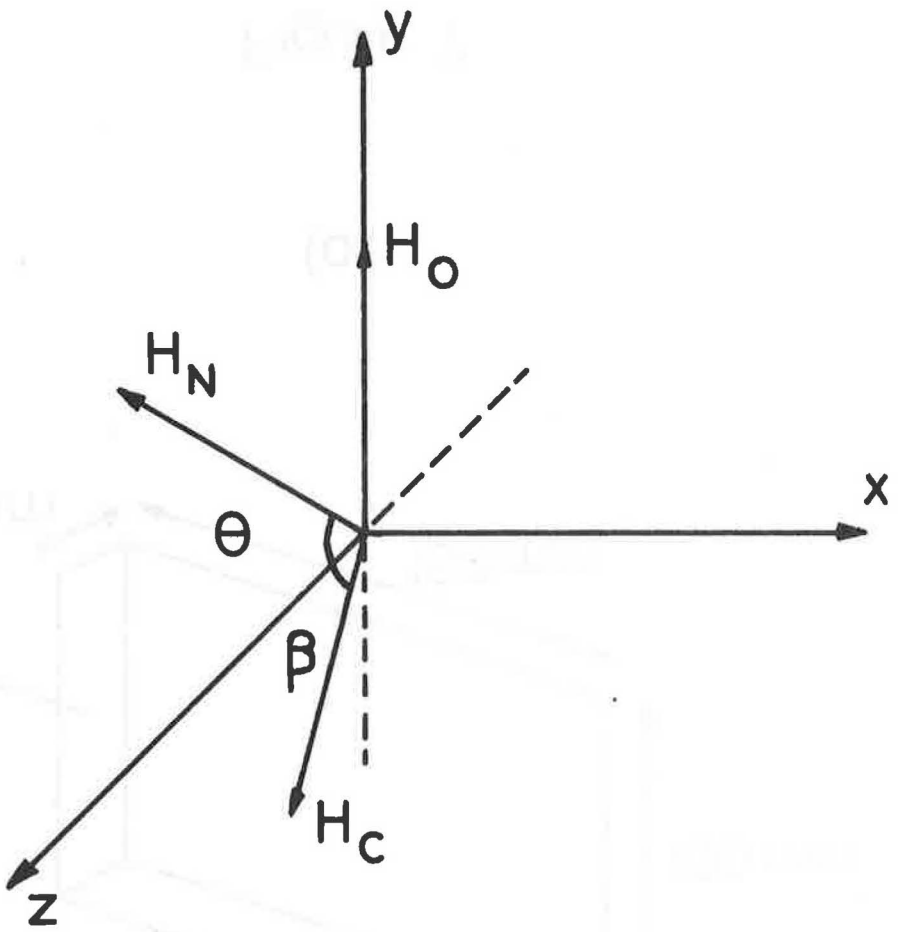

(b)

Figure 7

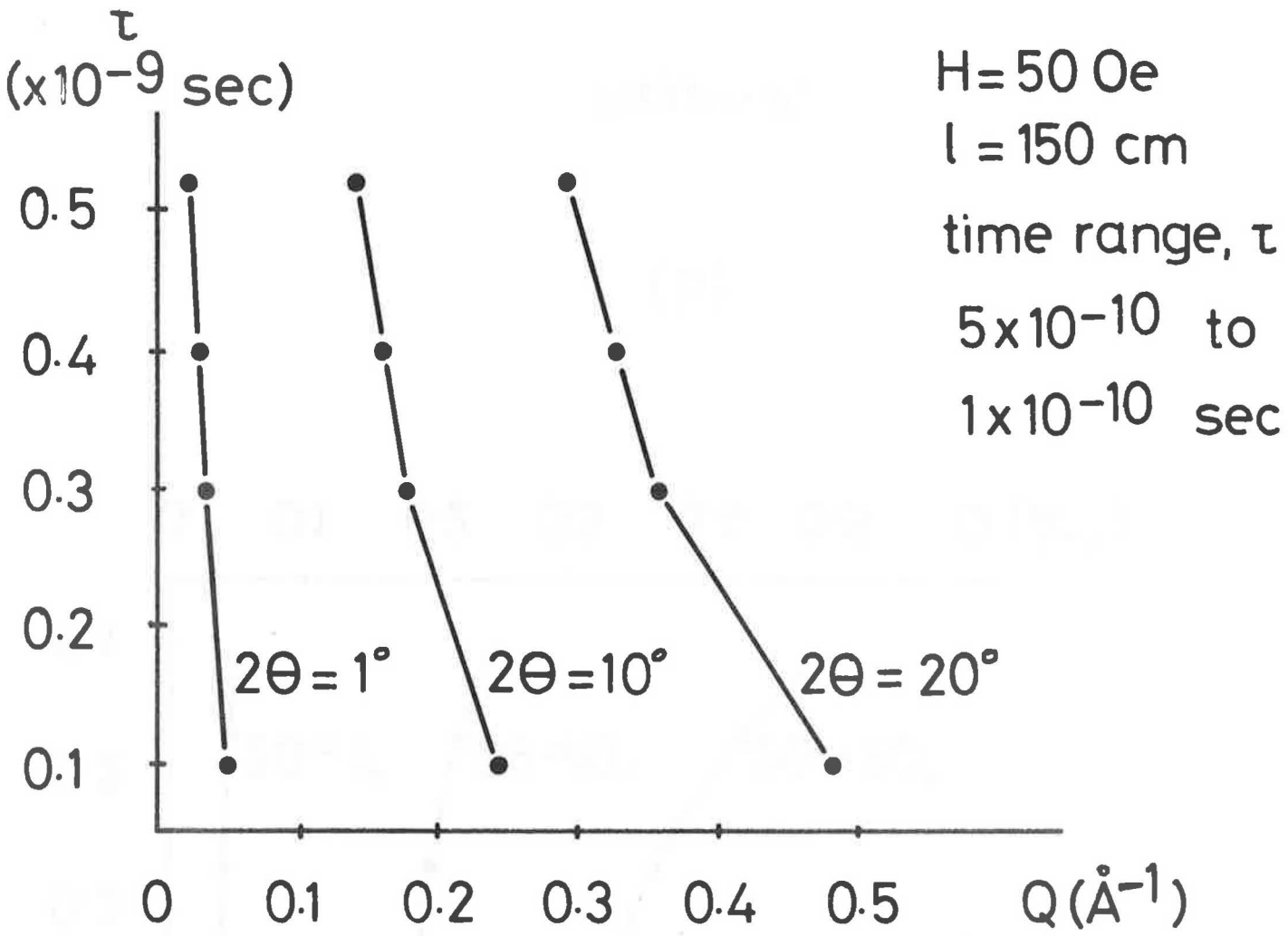
τ
(x10⁻⁹ sec)
0·5
0·4
0·3
0·2
0·1
H= 50 Oe
l = 150 cm
time range, τ
5x10⁻¹⁰ to
1x10⁻¹⁰ sec
2Θ = 1°
2Θ = 10°
2Θ = 20°
0
0·1
0·2
0·3
0·4
0·5
Q (Å⁻¹)

(a)

Figure 8

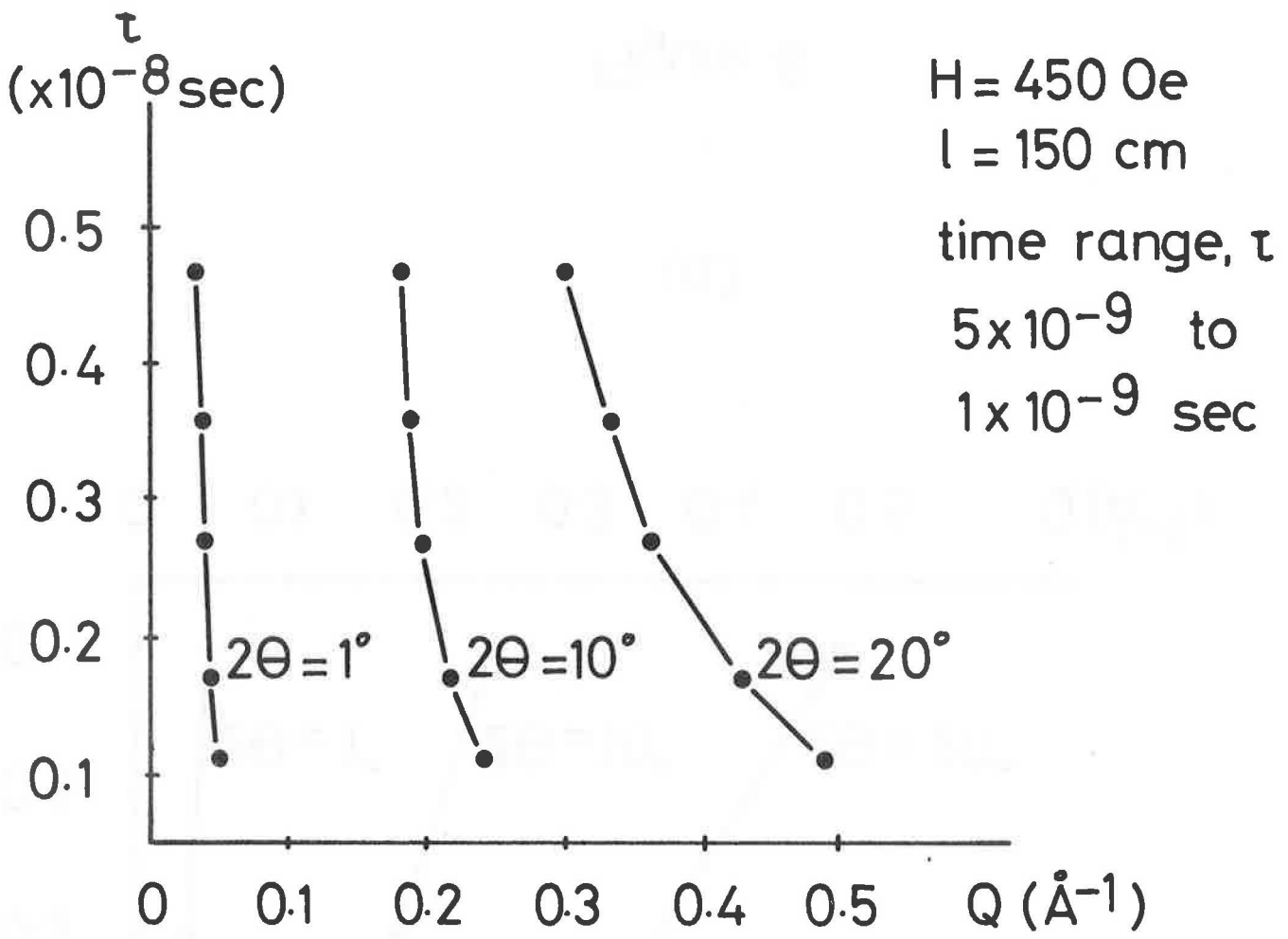
τ
(x10⁻⁸ sec)
H = 450 Oe
l = 150 cm
time range, τ
5x10⁻⁹ to
1x10⁻⁹ sec
0·5
0·4
0·3
0·2
0·1
2Θ = 1°
2Θ = 10°
2Θ = 20°
0
0·1
0·2
0·3
0·4
0·5
Q (Å⁻¹)

(b)

Figure 8

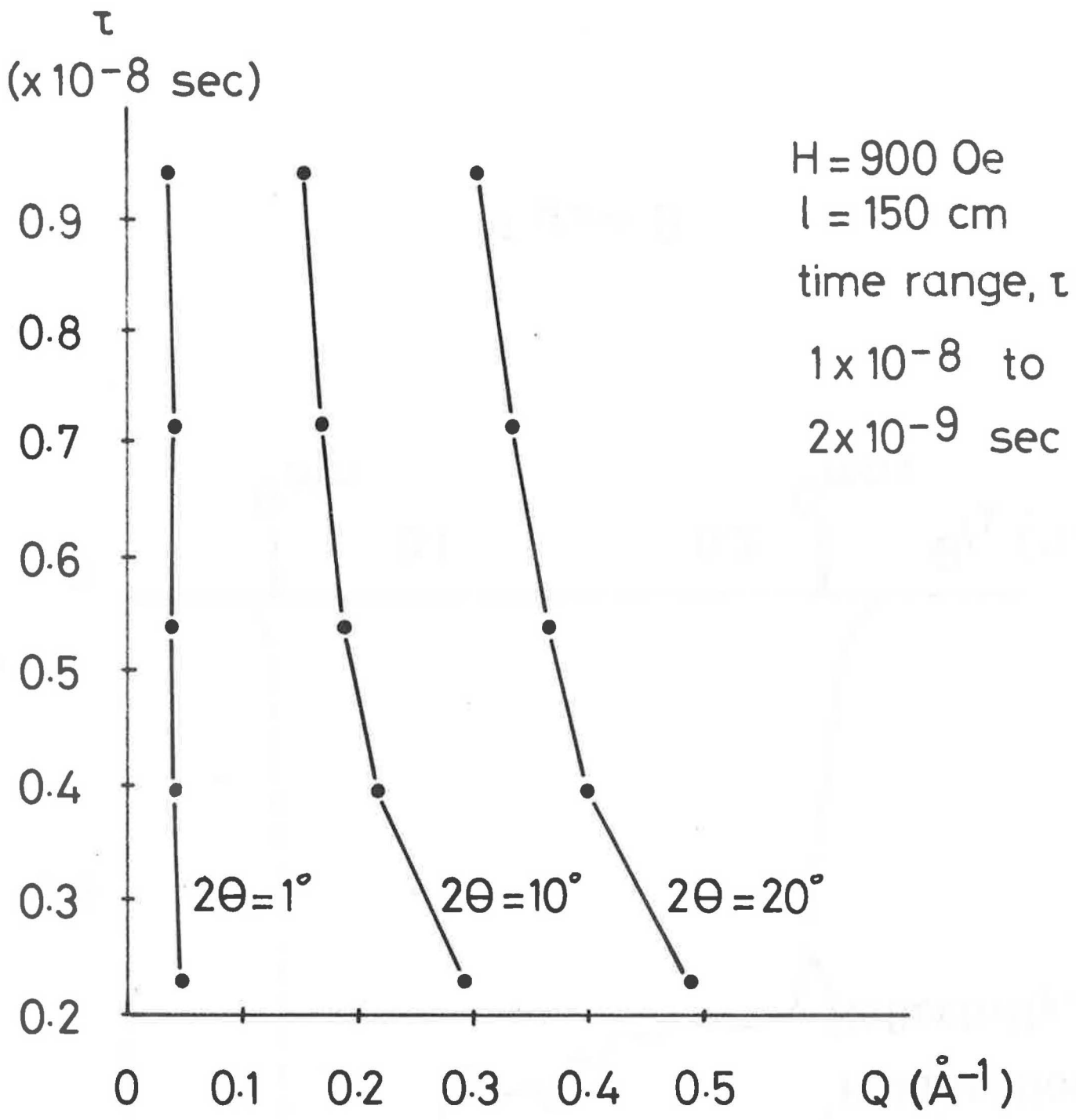
τ
(x 10⁻⁸ sec)
0·9
0·8
0·7
0·6
0·5
0·4
0·3
0·2
H = 900 Oe
l = 150 cm
time range, τ
1 x 10⁻⁸ to
2 x 10⁻⁹ sec
2Θ = 1°
2Θ = 10°
2Θ = 20°
0
0·1
0·2
0·3
0·4
0·5
Q (Å⁻¹)

(c)

Figure 8

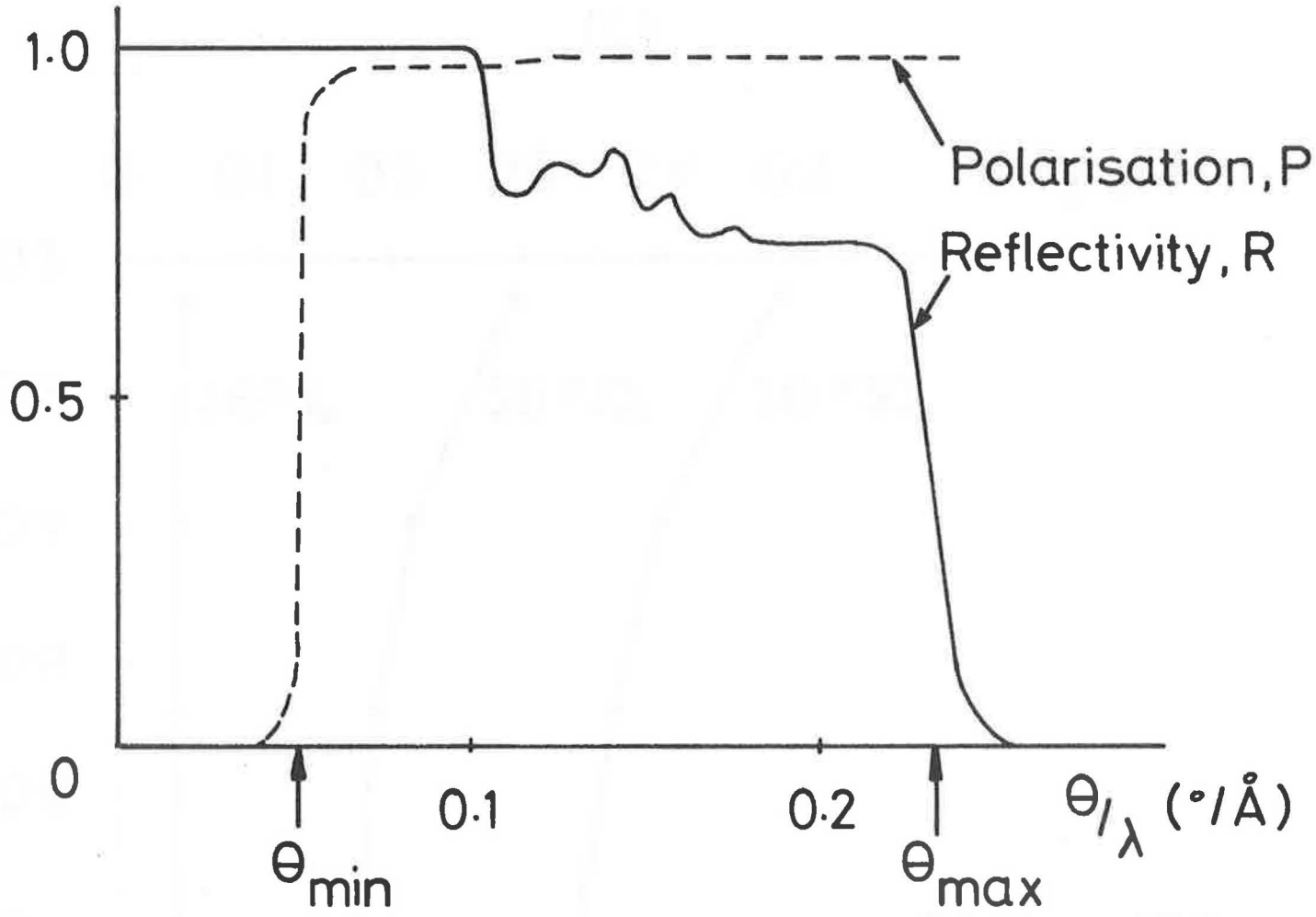

Figure 9

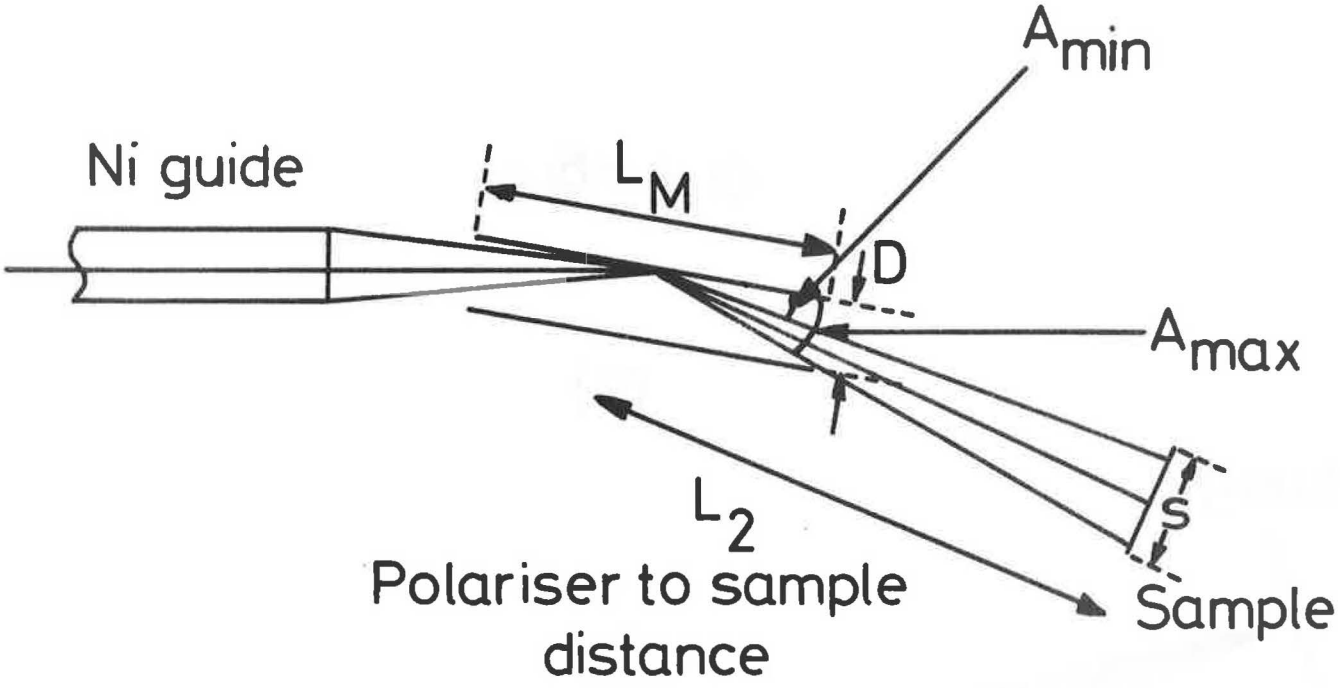
A_{min}
Ni guide
L_M
D
A_{max}
S
L_2
Polariser to sample distance
Sample

(a)

Figure 10

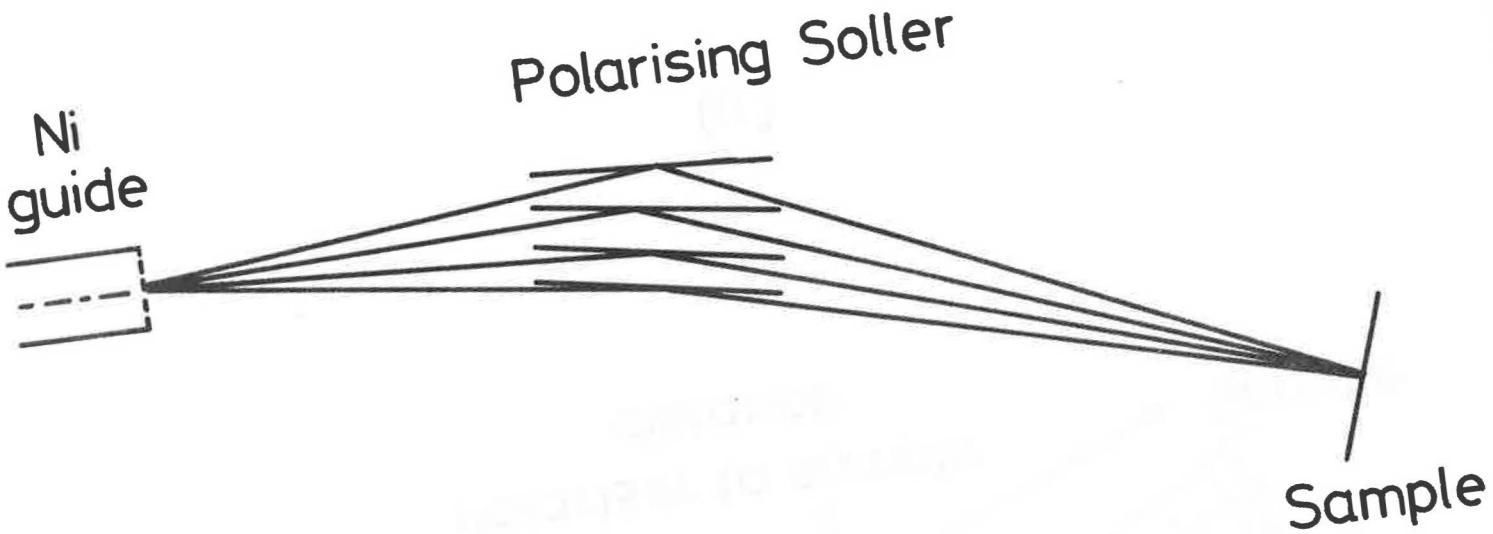

(b)

Figure 10

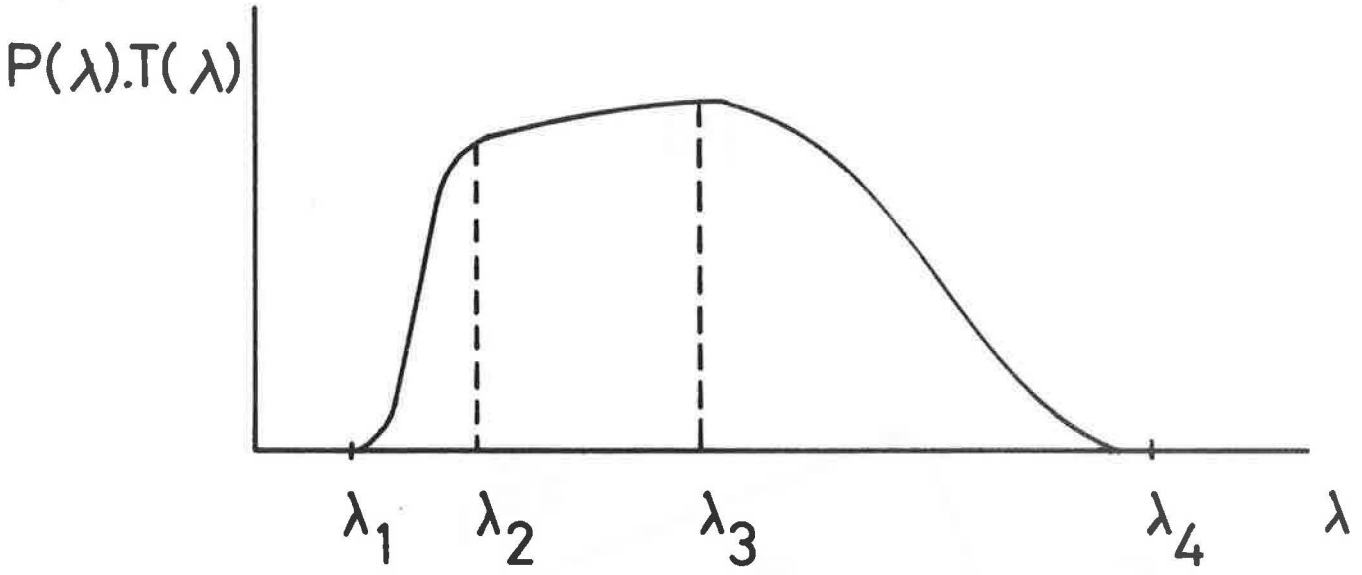

Figure 11

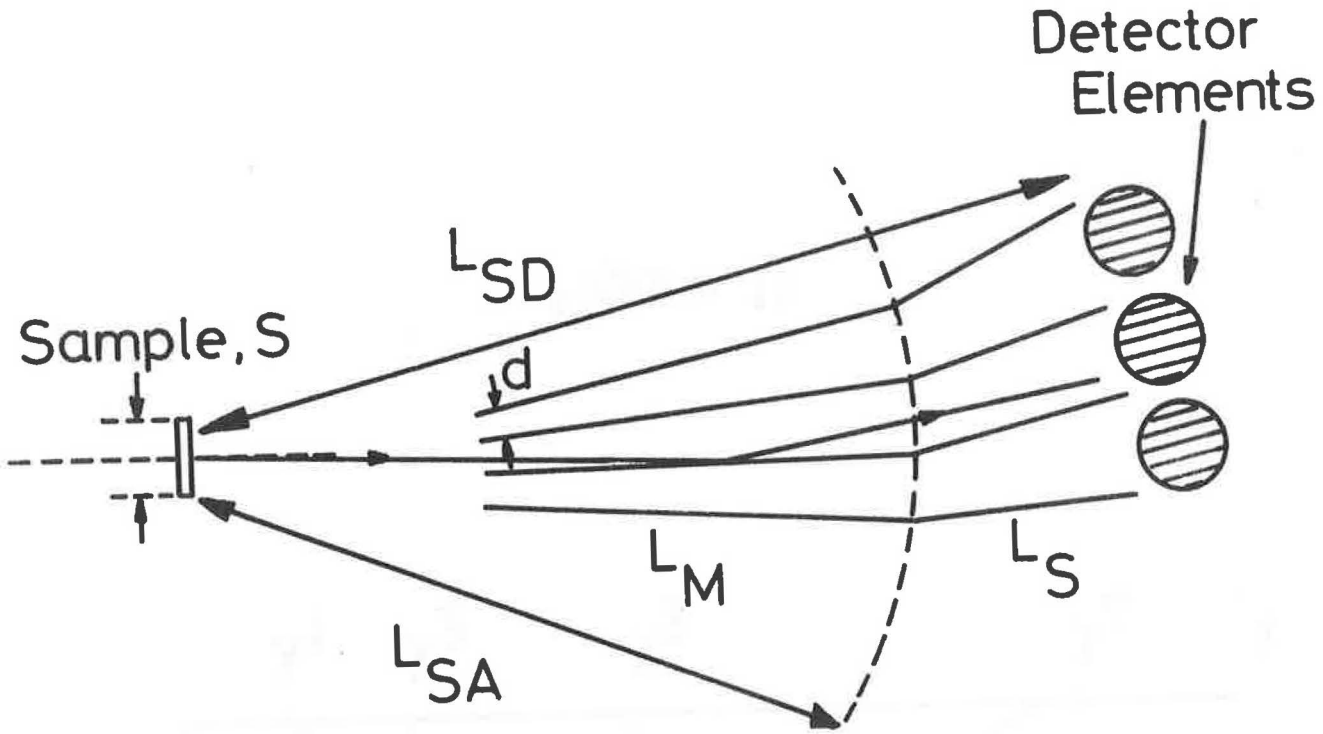

(a)

Figure 12

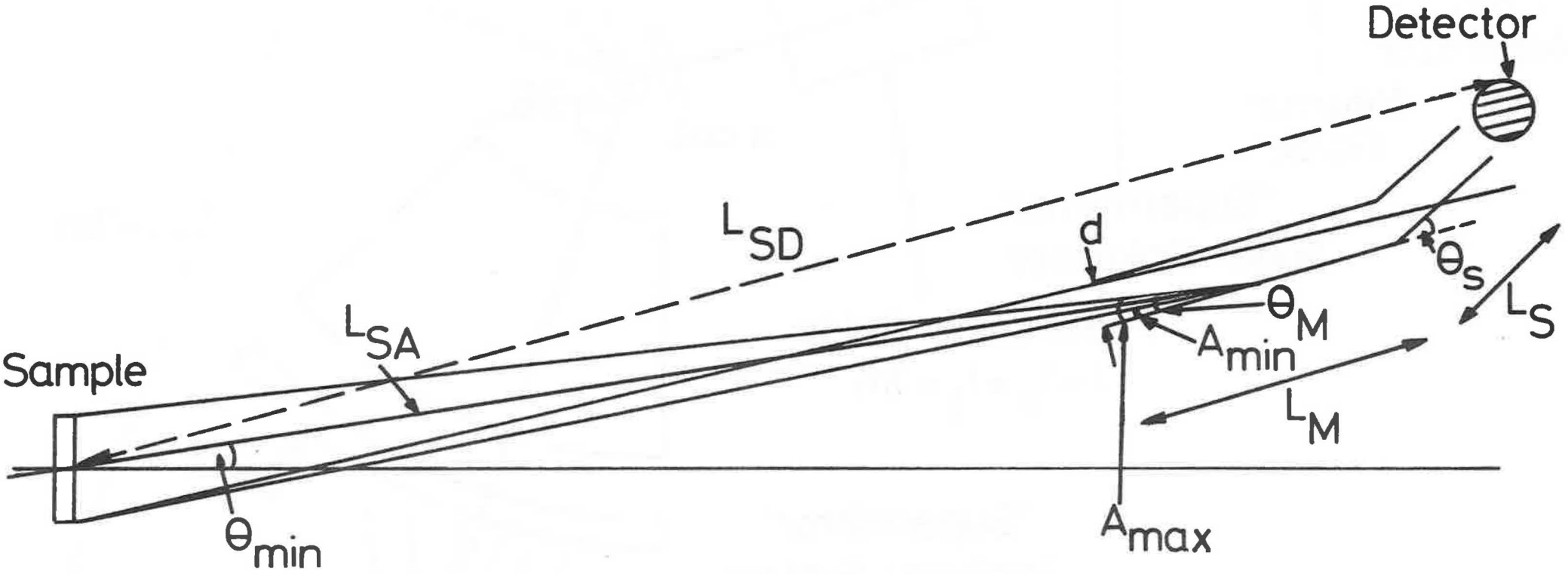
Detector
L_{SD}
d
θ_s
L_S
θ_M
L_{SA}
Sample
A_{min}
L_M
θ_{min}
A_{max}

(b)

Figure 12

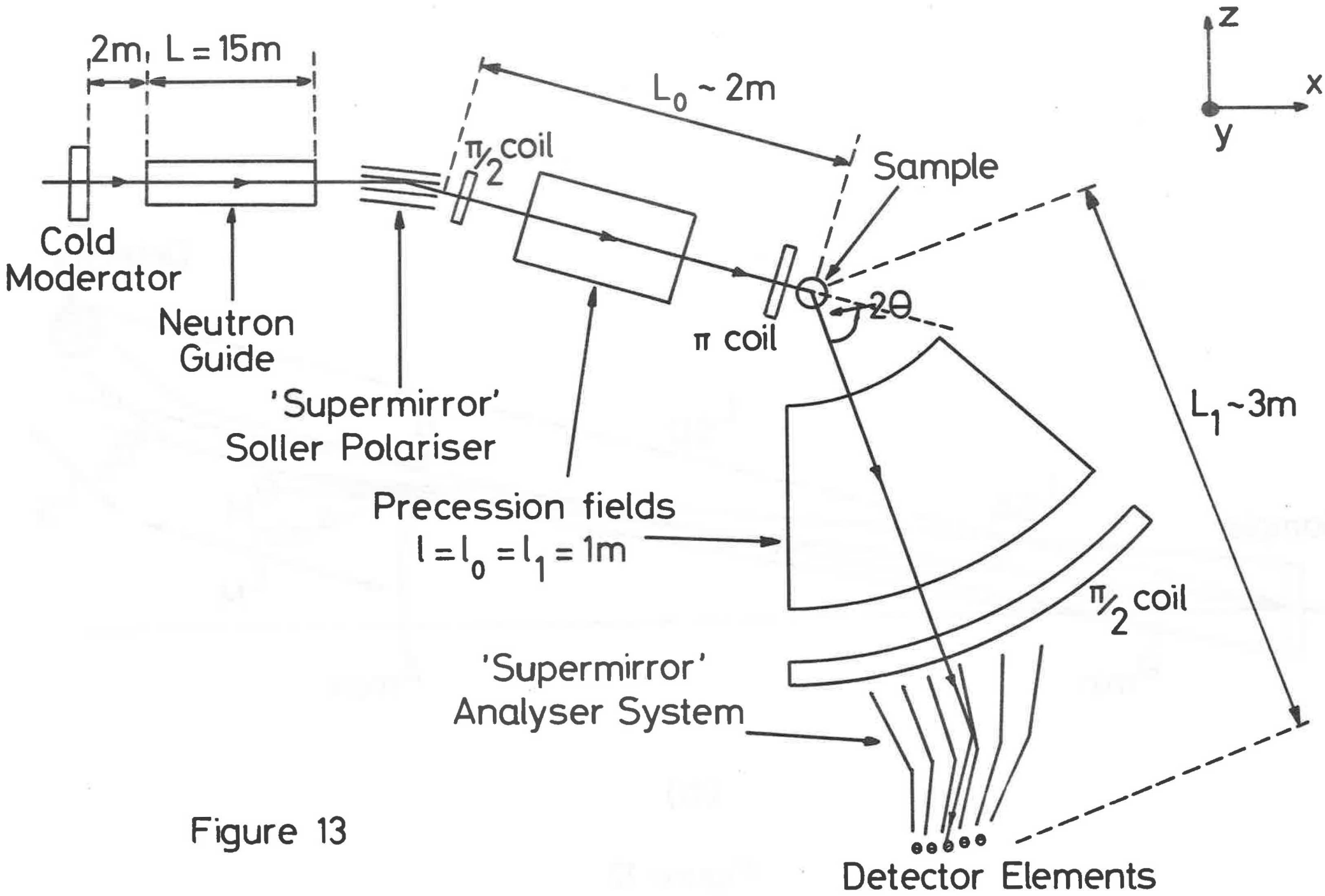
2m, L = 15m
$L_0 \sim 2m$
z
x
y
$\pi/2$ coil
Sample
Cold Moderator
Neutron Guide
'Supermirror' Soller Polariser
π coil
2θ
$L_1 \sim 3m$
Precession fields
$l = l_0 = l_1 = 1m$
$\pi/2$ coil
'Supermirror' Analyser System
Detector Elements

Figure 13